

Representation of phosphorus cycle in Joint UK Land Environment Simulator (vn5.5_JULES-CNP)

Mahdi (André) Nakhavali¹, Lina M. Mercado^{1,2}, Iain P. Hartley¹, Stephen Sitch¹, Fernanda V Cunha³, Raffaello di Ponzio³, Laynara F. Lugli³, Carlos A. Quesada³, Kelly M. Andersen^{1,4,5}, Sarah E. Chadburn⁶, Andy J. Wiltshire^{1,7}, Douglas B. Clark², Gyovanni Ribeiro³, Lara Siebert³, Anna C. M. Moraes³, Jéssica Schmeisk Rosa³, Rafael Assis³ and José L. Camargo³

¹University of Exeter, College of Life and Environmental Sciences, Exeter, EX4 4QE, United Kingdom

²UK Centre for Ecology and Hydrology, Wallingford, OX10 8BB, United Kingdom

³Coordination of Environmental Dynamics, National Institute of Amazonian Research, Manaus, AM 69060-062, Brazil

⁴University of Edinburgh, School of Geosciences, Edinburgh, EH8 9AB, UK

⁵Nanyang Technological University, Asian School of the Environment, Singapore, 639798, Singapore

⁶College of Engineering, Mathematics, and Physical Sciences, University of Exeter, Exeter, EX4 4QE, United Kingdom

⁷Met Office Hadley Centre, Exeter, Devon, EX1 3PB, United Kingdom

Correspondence to: Mahdi (André) Nakhavali (m.nakhavali@exeter.ac.uk)

Abstract

Most Land Surface Models (LSMs), the land components of Earth system models (ESMs), include representation of [nitrogen \(N\)](#) limitation on ecosystem productivity. However only few of these models have incorporated phosphorus (P) cycling. [In topical ecosystems, this is likely to be important](#) as N tends to be abundant but the availability of rock-derived elements, such as P, can be very low. Thus, without a representation of P cycling, tropical forest response in areas such as Amazonia to rising atmospheric CO₂ conditions remains highly uncertain. In this study, we introduced P dynamics and its interactions with the N and carbon (C) cycles into the Joint UK Land Environment Simulator (JULES). The new model (JULES-CNP) includes the representation of P stocks in vegetation and soil pools, as well as key processes controlling fluxes between these pools. [We evaluate JULES-CNP using in situ data collected at a low fertility site in the Central Amazon, with a soil P content representative of 60% of soils across the Amazon basin, to parameterise, calibrate and evaluate JULES-CNP. Novel soil and plant P pool observations are used for parameterisation and calibration and the model is evaluated against C fluxes and stocks, and for those soil P pools not used for parameterisation/calibration. We then apply the model under elevated CO₂ \(600 ppm\) at our study site to quantify the impact of P limitation on CO₂ fertilization. We compare our results against current state of the art CNP models using the same methodology that was used in the AmazonFACE model intercomparison study.](#) The model is able to reproduce the observed plant and soil P pools and fluxes [used for evaluation](#) under ambient CO₂. We estimate P to limit net primary productivity (NPP) by 24% under current CO₂ and by 46% under elevated CO₂. Under elevated CO₂, biomass in simulations accounting for CNP increase by 10% relative to at contemporary CO₂, although it is 5% lower compared with CN and C-only simulations. Our results highlight the potential for high P limitation and therefore lower CO₂ fertilization capacity in the Amazon forest with low fertility soils.

1. Introduction

Land ecosystems currently take up about 30% of anthropogenic CO₂ emissions (Friedlingstein *et al.*, 2020), thus buffering the anthropogenic increase in atmospheric CO₂. Tropical forests play a major role in the land C cycle, account for about half of global [net primary production](#) (NPP)(Schimel *et al.*, 2015), and store the highest above ground carbon among all biomes (Pan *et al.*, 2011; Mitchard, 2018).

The C sink capacity of tropical forests may be constrained by nutrient availability for plant photosynthesis and growth (Vitousek and Howarth, 1991; Elser *et al.*, 2007; LeBauer and Treseder, 2008) via either P (Nordin, Högberg and Näsholm, 2001; Shen *et al.*, 2011) and N related processes (DeLuca, Keeney and McCarty, 1992; Perakis and Hedin, 2002). Global process-based models of vegetation dynamics and function suggest a continued land C sink in the tropical forests, largely attributed to the CO₂ fertilization effect (Sitch *et al.*, 2008; Schimel, Stephens and Fisher, 2015; Koch, Hubau and Lewis, 2021). However, many of these models typically do not consider P constraints on plant growth (Fleischer *et al.*, 2019), which is likely to be an important limiting nutrient in tropical ecosystems, characterised by old and heavily weathered soils. The importance of nutrient cycling representation in Earth System Models (ESMs), and the lack thereof, was highlighted by Hungate *et al.* (2003) and Zaehle and Dalmonech (2011), showing the significance of [nitrogen](#) inclusion in ESMs for generating more realistic estimations of the future evolution of the terrestrial C sink. However, in the Coupled Climate C Cycle Model Inter-comparison Project (C4MIP), none of the participating ESMs included N dynamics (Friedlingstein *et al.*, 2006). Seven years later, for the update in CMIP5 (Anav *et al.*, 2013), three models out of eighteen with [N dynamics were included](#) (Bentsen *et al.*, 2013; Long *et al.*, 2013; Ji *et al.*, 2014). Although much progress has been made in the inclusion of an N cycle in ESMs so far, none of the CMIP5 models included P cycling and in the most recent CMIP6, only one model includes P (ACCESSESM1.5 model) (Arora *et al.*, 2020).

The long history of soil development in tropical regions which involves the loss of rock-derived nutrients through weathering and leaching on geologic timescales (Vitousek *et al.*, 1997, 2010) results in highly weathered soils. Soil P is hypothesized to be among the key limiting nutrients to plant growth in tropical forests (Vitousek *et al.*, 1997, 2010; Hou *et al.*, 2020), unlike temperate forest where N is hypothesised to be the main constraint (Aerts and Chapin, 1999; Luo *et al.*, 2004). Low P availability in tropical soils is related to the limited un-weathered parent material or organic compounds as source of P (Walker and Syers, 1976), active sorption (Sanchez, 1977) and high occlusion (Yang and Post, 2011) which further reduce plant available P. [Although N limitation can impact the terrestrial C sink response to increasing atmospheric CO₂ by changing plant C fixation capacity \(Luo *et al.*, 2004\), this can be partially ameliorated over time by input of N into the biosphere via the continuous inputs of N into ecosystems from atmospheric deposition and biological N fixation \(Vitousek *et al.*, 2010\). P-limitation is pervasive in natural ecosystems \(Hou *et al.*, 2020\) and the lack of large P inputs into ecosystems, especially those growing on highly weathered soil, may make P limitation a stronger constraint on ecosystem response to elevated CO₂ \(eCO₂\) than N \(Gentile *et al.*, 2012; Sardans, Rivas-Ubach and Peñuelas, 2012\).](#) This causes considerable uncertainty in predicting the future of the Amazon forest C sink (Yang *et al.*, 2014).

There is evidence to suggest P limitation on plant productivity in the Amazon forest (Malhi, 2012) where it has been shown that the younger, more fertile west and south-west Amazon soils have higher tree turnover (Phillips *et al.*, 2004; Stephenson and Van Mantgem, 2005) and stem growth rates (Malhi *et al.*, 2004) and lower above ground biomass (Baker *et al.*, 2004; Malhi *et al.*, 2006) compared to their central and eastern counterparts. Total soil P has been found as the best predictor of stem growth (Quesada *et al.*, 2010) and of total NPP (Aragão *et al.*, 2009) across this fertility gradient, and foliar P is positively related to plant photosynthetic capacity (V_{cmax} and J_{cmax}) in these forests (Mercado *et al.*, 2011).

However, modelling studies are unable to reproduce observed spatial patterns of NPP and biomass in the Amazon due to missing [information on nutrient availability and soil fertility impact on productivity \(Wang, Law and Pak, 2010; Vicca *et al.*, 2012; Yang *et al.*, 2014\)](#) and due to the lack of inclusion of soil P constraints on plant productivity and function. [Nevertheless, some modelling works have](#) focused on improving process and parameter representation using the observational data of spatial variation in woody biomass residence time (Johnson *et al.*, 2016), soil texture and soil P to parameterise the maximum RuBiCo carboxylation capacity (V_{cmax}) (Castanho *et al.*, 2013). Results from these studies successfully represent observed patterns of Amazon forest biomass growth increases with increasing soil fertility. However, the full representation of these interactions and the impact of the soil nutrient availability on biomass productivity is still missing in most of ESMs.

104 So far, several dynamic global vegetation models have been developed to represent P cycling within the soil
105 (Yang *et al.*, 2013; Haverd *et al.*, 2018) and between plant and soils for tropical forests particularly (Yang *et al.*,
106 2014; Zhu *et al.*, 2016; Goll *et al.*, 2017). Furthermore, a comprehensive study included several models with C-
107 N-P cycling and their feedbacks on the atmospheric C fixation and biomass growth in Amazon forests under
108 ambient and eCO₂ conditions (Fleischer *et al.*, 2019). Despite these developments, data to underpin them and
109 their projections, particularly for the tropics, is sparse and remains challenging particularly for the Amazon
110 forest (Reed *et al.*, 2015; Jiang *et al.*, 2019). Moreover, due to the lack of detailed measurements, the P-related
111 processes such as ad/desorption and uptake represented in these models are under-constrained and likely
112 oversimplified, thus the future predictions of Amazon forest responses to eCO₂ and climate change are
113 uncertain. To fill this gap, in this study, we will use data collected as part of the Amazon Fertilization
114 Experiment (AFEX), the first project that focuses on experimental soil nutrient manipulation in the Amazon,
115 with a comprehensive data collection program covering plant ecophysiology, C stocks and fluxes, soil processes
116 including P stocks. Thus, our model parameterization compared to prior P modelling studies includes detailed P
117 processes representation using the site measurements.

118
119 Here, we describe the development and implementation of the terrestrial P cycle in the Joint UK Land
120 Environment Simulator (JULES) (Clark *et al.*, 2011), the land component of the UK Earth System Model
121 (UKESM), following the structure of the prior N cycle development (Wiltshire *et al.*, 2021). The model
122 (JULES-CNP) is parameterized and calibrated using novel in situ P soil and plant data from a well-studied forest
123 site in Central Amazon near to Manaus, Brazil with soil P content representative of 60% of soils across the
124 Amazon basin. We then evaluate the model against carbon stocks and fluxes from data sets from our study site
125 and the nearby K34 field site. To test the model, we followed the protocol of Fleischer *et al.*, (2019), to predict
126 nutrient limitations on land biogeochemistry under ambient and eCO₂. Predictions of the CO₂ fertilization effect
127 in JULES-CNP are compared to those in current versions of the model with coupled C and N cycles (JULES-
128 CN) and with C cycle only (JULES-C).

129
130

131 2. Material and methods

132
133

133 2.1 JULES

134
135

135 JULES is a process-based model that integrates water, energy, C cycling (JULES-C) (Clark *et al.*, 2011) and N
136 cycling (JULES-CN) (Wiltshire *et al.*, 2021) between the atmosphere, vegetation and soil (Best *et al.*, 2011;
137 Clark *et al.*, 2011). Vegetation dynamics are represented in JULES using the TRIFFID model, using nine
138 distinct plant functional types (PFTs) (tropical and temperate broadleaf evergreen trees, broadleaf deciduous
139 trees, needle-leaf evergreen and deciduous trees, C3 and C4 grasses, and evergreen and deciduous shrubs), as
140 well as height competition (Harper *et al.*, 2016). JULES simulates Gross Primary Productivity (GPP) based on a
141 coupled photosynthesis and water balance scheme, from which autotrophic respiration for each living tissue
142 (leaf, wood, root) is subtracted to estimate NPP. In JULES we assume a process-based leaf-level photosynthesis
143 scaled up to the canopy. Therefore, in JULES CNP in order to keep consistency with JULES C-CN, we also
144 assume a multi-level canopy, and leaf N and P in exponentially decreases through the canopy (CanRadMod 6)
145 (Clark *et al.*, 2011). NPP is then allocated to increase tissue C stocks and to spread, i.e., expand the fractional
146 coverage of the PFT. The resultant PFT fractional coverages depend in addition on competition across PFTs for
147 resources, e.g., light. Tissue turnover and vegetation mortality add C into the litter pools. Representation of soil
148 organic C (SOC) follows the RothC equations (Jenkinson *et al.*, 1990; Jenkinson and Coleman, 2008) defining
149 four C pools: decomposable plant material (DPM) and resistant plant material (RPM), which receive direct input
150 from litterfall, and microbial biomass (BIO) and humified material (HUM) which receive a fraction of
151 decomposed C from DPM and RPM which is not released to the atmosphere. The limitation of N on SOC is
152 applied to the vegetation and soil components using a dynamic C:N ratio to modify the mineralization and
153 immobilization processes as described in Wiltshire *et al.*, (2021). Note that the soil component of JULES-CN
154 can be run either as a single box model or vertically resolved over soil depth (JULES-CN layered), and in this
155 paper we build upon the vertically resolved version described in Wiltshire *et al.* (2021).

156
157

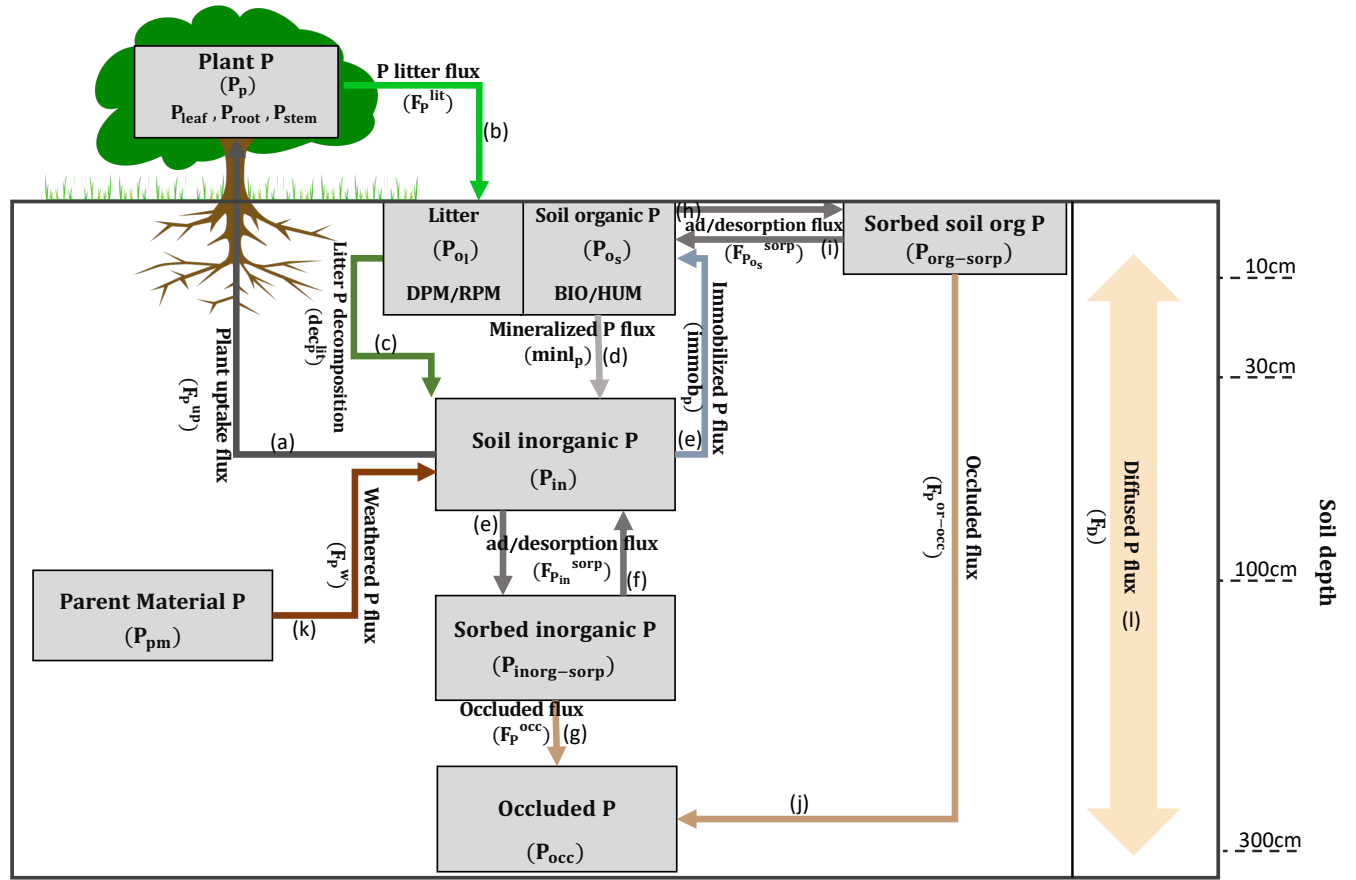
157 2.2 JULES-CNP

158
159

159 JULES-CNP includes the representation of the P cycle in JULES version (vn5.5). It includes P fluxes within the
160 vegetation and soil components, and the specification of P pools and processes related to P cycling within the
161 soil column (Figure.1). A parent material pool is introduced to consider the input of weathered P. The adsorbed,
162 desorbed and occluded fractions of P for both organic and inorganic P are also represented. However, except for
163 parent material and occluded P pools, all other pools are estimated at each soil layer. The description of changes

164
165
166
167
168

in pools and associated relative fluxes are explained in detail in the next sections. [However, despite JULES-CN that includes N leaching and deposition, P leaching and deposition are omitted in the current version of JULES-CNP.](#)



169
170

Figure.1 – JULES CNP model scheme

171
172
173

2.2.1 P pools

JULES represents eight P pools comprising organic and inorganic P: in plant P (P_p) and soil pools (in each soil layer (n)): litter P (P_{ol}), soil organic P (P_{os}), soil inorganic P (P_{in}), organic sorbed ($P_{org-sorp}$), inorganic sorbed ($P_{inorg-sorp}$), [parent material](#) (P_{pm}) and occluded (P_{occ}) P comprised of both organic and inorganic P. All pools are in units of $kg P m^{-2}$ (Fig 1, Tables 1 and 2).

Plant P pool is composed of leaf (P_{leaf}), fine root (P_{root}) and stem together with coarse root (P_{stem}), which are related to their associated C pools (C_{leaf} , C_{root} , C_{stem}) in ($kg C m^{-2}$) and [fixed](#) C to P ratios ($C:P_{leaf}$, $C:P_{root}$, $C:P_{stem}$) as follows:

$$P_{leaf} = \frac{C_{leaf}}{C:P_{leaf}} \quad (eq.1)$$

$$P_{root} = \frac{C_{root}}{C:P_{root}} \quad (eq.2)$$

$$P_{stem} = \frac{C_{stem}}{C:P_{stem}} \quad (eq.3)$$

Therefore, the plant P pool (P_p) is the sum of all vegetation P pools as follows:

$$P_p = P_{leaf} + P_{root} + P_{stem} \quad (eq.4)$$

191
192

193 [Description of the plant P pool \(\$P_p\$ \) follows Zhu *et al.*, \(2016\) and](#) is estimated as the difference between the
 194 input, plant uptake F_p^{up} (eq.26) and output of this pool, plant litter flux F_p^{lit} (eq.28), with both fluxes
 195 expressed in kg P m⁻² yr⁻¹ as follows:

$$197 \frac{dP_p}{dt} = F_p^{up} - F_p^{lit} \quad (\text{eq.5})$$

198 The litter P pool (P_{Ol}) is estimated as a sum of P_{DPM} and P_{RPM} pools. Each pool is formed by the fluxes of plant
 199 litter input (F_p^{lit}) and the outgoing decomposed P (dec_p^{lit}) both expressed in kg P m⁻² yr⁻¹ (eq.28-29).
 200 Furthermore, the plant litter input is modified based on the plant type material ratio α (in order to distribute the
 201 litter input based on the DPM/RPM fraction) as follows:

$$204 \frac{dP_{DPM}}{dt} = F_{P_n}^{lit} \times \alpha - dec_{P_{DPM},n} \quad (\text{eq.6})$$

$$206 \frac{dP_{RPM}}{dt} = F_{P_n}^{lit} \times (1 - \alpha) - dec_{P_{RPM},n} \quad (\text{eq.7})$$

$$208 P_{Ol} = \sum_{n=1}^N P_{DPM,n} + \sum_{n=1}^N P_{RPM,n} \quad (\text{eq.8})$$

210 The soil organic pool (P_{Os}) is represented as the sum of P_{BIO} and P_{HUM} . These pools are estimated from the
 211 difference between P inputs from [total immobilized \(\$F_{immob_p}\$ \) distributed between BIO and HUM based on](#)
 212 [fixed fraction \(0.46 for BIO, 0.54 for HUM\) \(Jenkinson *et al.*, 1990; Jenkinson and Coleman, 2008\)](#) and
 213 desorbed P $F_{P_{Os}}^{desorp}$ and P outputs from mineralized (F_{minl_p}), and adsorbed P fluxes ($F_{P_{Os}}^{sorp}$) (adsorption:
 214 eq. 40 and desorption: eq.41) with all fluxes expressed in kg P m⁻² yr⁻¹ as follows:

$$216 \frac{dP_{BIO}}{dt} = 0.46 \times F_{immob_{P_n}} + F_{P_{Os_{BIO},n}}^{desorp} - F_{minl_{P_{BIO},n}} - F_{P_{Os_{BIO},n}}^{sorp} \quad (\text{eq.9})$$

$$218 \frac{dP_{HUM}}{dt} = 0.54 \times F_{immob_{P_n}} + F_{P_{Os_{HUM},n}}^{desorp} - F_{minl_{P_{HUM},n}} - F_{P_{Os_{HUM},n}}^{sorp} \quad (\text{eq.10})$$

$$220 P_{Os} = \sum_{n=1}^N P_{BIO,n} + \sum_{n=1}^N P_{HUM,n} \quad (\text{eq.11})$$

223 [Description of the inorganic sorbed P pool \(\$P_{inorg-sorp}\$ \) follows Wang *et al.*, \(2007\) and](#) is represented as the
 224 difference between the input flux of inorganic sorption ($F_{P_{in}}^{sorp}$) (eq. 37) and output fluxes of inorganic
 225 desorption ($F_{P_{in}}^{desorp}$) (eq. 38) and occluded P (F_p^{occ}) (eq. 39), with all fluxes expressed in kg P m⁻² yr⁻¹ as
 226 follows:

$$228 \frac{dP_{inorg-sorp}}{dt} = \sum_{n=1}^N F_{P_{in,n}}^{sorp} - \sum_{n=1}^N F_{P_{in,n}}^{desorp} - \sum_{n=1}^N F_{P_n}^{occ} \quad (\text{eq.12})$$

230 [Describing of the occluded \(\$P_{occ}\$ \) P pool follows Wang *et al.*, \(2007\) and Hou *et al.*, \(2019\) and](#) is represented
 231 as the sum of input fluxes of occluded P from both organic (F_p^{or-occ}) (eq. 42) and inorganic P pools (F_p^{occ})
 232 expressed in kg P m⁻² yr⁻¹, as follows:

$$234 \frac{dP_{occ}}{dt} = \sum_{n=1}^N F_{P_n}^{occ} + \sum_{n=1}^N F_{P_n}^{or-occ} \quad (\text{eq.13})$$

236 [Describing of the organic sorbed P pool \(\$P_{org-sorp}\$ \) follows Wang *et al.*, \(2007\) and](#) is represented as the
 237 difference between the input flux of organic sorption ($F_{P_{Os_n}}^{sorp}$) and output fluxes of organic desorption
 238 ($F_{P_{Os_n}}^{desorp}$) and occluded P (F_p^{occ}), with all fluxes expressed in kg P m⁻² yr⁻¹ as follows:

$$240 \frac{dP_{org-sorp}}{dt} = \sum_{n=1}^N F_{P_{Os_n}}^{sorp} - \sum_{n=1}^N F_{P_{Os_n}}^{desorp} - \sum_{n=1}^N F_{P_n}^{or-occ} \quad (\text{eq.14})$$

244 [Describing of P from parent material \(\$P_{pm}\$ \) pool follows Wang *et al.*, \(2007\) and depends on the weathering](#)
 245 [flux \(\$F_p^w\$ \) \(eq. 43\) in kg P m⁻² yr⁻¹ as follows:](#)

$$247 \frac{dP_{pm}}{dt} = - \sum_{n=1}^N F_{P_n}^w \quad (\text{eq.15})$$

250 2.2.2. [C and P fluxes](#)

251
 252 [NPP in JULES is calculated as the difference between GPP and autotrophic respiration. In JULES-CNP,](#)
 253 [potential NPP represent the amount of C, available for tissue growth \(C density increase\) on a unit area, and](#)
 254 [spreading \(vegetation cover increase as a result of reproduction and recruitment\), ie to increase the area covered](#)
 255 [by the vegetation type, assuming no nutrient limitation. The reported NPP in the literature often includes other C](#)
 256 [fluxes related to the exudates, volatiles production and non-structural carbohydrates \(Malhi *et al.*, 2009; Chapin](#)
 257 [et al., 2011; Walker *et al.*, 2021\) which are challenging to measure \(Malhi, Doughty and Galbraith, 2011\).](#)
 258 [Therefore, actual NPP is for our purposes equal to Biomass Production \(BP\), and is calculated as potential NPP](#)
 259 [minus excess C \(lost to the plant through autotrophic respiration\), with the latter the C that cannot be used to](#)
 260 [growth new plant tissue due to insufficient plant nutrient supply. Hence, if the system is limited by the](#)
 261 [availability of N and/or P, NPP will be adjusted to match the growth that can be supported with the limited N or](#)
 262 [P supply, with any excess carbohydrate lost through excess C.](#)

263 The total excess C term (ψ_t) (kg C m⁻² yr⁻¹) is calculated as:

$$265 \psi_t = \psi_g + \psi_s \quad (\text{eq.16})$$

266 where ψ_g and ψ_s are the [excess C fluxes](#) due to growth (g) and spread (s) and are assumed to be rapidly respired
 267 by plants.

268
 269 [Therefore, BP is calculated as the difference between potential NPP \(\$\Pi_c\$ \) and total excess C:](#)

$$272 BP = \Pi_c - \psi_t \quad (\text{eq.17})$$

273
 274 [The litter production in JULES before limitation is estimated based on the as follows:](#)

$$276 F_{C_n}^{lit} = \gamma_{leaf} C_{leaf} + \gamma_{root} C_{root} + \gamma_{wood} C_{wood} \quad (\text{eq.18})$$

277
 278 [where \$\lambda\$ is the leaf, root and stem re-translocation \(at daily timestep\) coefficient \(Clark *et al.*, 2011\) and \$\gamma\$ is a](#)
 279 [temperature dependent turnover rate representing the phenological state \(Clark *et al.*, 2011\). P limitation is](#)
 280 [applied on the C litter production similar to the N scheme of JULES \(JULES-CN\) \(Wiltshire *et al.*, 2021\). In](#)
 281 [JULES-CN the N limitation effect on the litter production is captured by estimating the available C for litter](#)
 282 [production as a difference between the NPP and excess C \(Wiltshire *et al.*, 2021\).](#)

283
 284 [Similar to other P-enabled models \(Yang *et al.*, 2014; Goll *et al.*, 2017\), JULES-CNP follows the same structure](#)
 285 [as its N model component. Description of the plant P and N demand follow Wang *et al.*, \(2007\) and are](#)
 286 [represented by the sum of demand \(\$\phi_t\$ \) to sustain growth \(P-related: \(\$\phi_{gP}\$ \), N-related: \(\$\phi_{gN}\$ \)\) and to sustain](#)
 287 [vegetation spreading \(to increment PFT fractional coverage\) \(P-related: \(\$\phi_{sP}\$ \), N-related: \(\$\phi_{sN}\$ \)\) and is](#)
 288 [expressed in \(P-related in kg P m⁻² yr⁻¹; N-related in kg N m⁻² yr⁻¹\). The total demand for growth \(\$\phi_g\$ \) and](#)
 289 [spreading \(\$\phi_s\$ \) is controlled by the dominant demand between P \(\$\phi_{gP}\$ \) and N \(\$\phi_{gN}\$ \) as follows:](#)

$$291 \phi_t = \phi_g + \phi_s \quad (\text{eq.19})$$

$$292 \phi_{gP} = \frac{P_p}{C_v} \left(\Pi_c - \frac{dC_v}{dt} - \psi_g \right) \quad (\text{eq.20})$$

$$293 \phi_{sP} = \frac{P_p}{C_v} \left(\Pi_c - \frac{dC_v}{dt} - \psi_s \right) \quad (\text{eq.21})$$

$$294 \phi_{gN} = \frac{N_v}{C_v} \left(\Pi_c - \frac{dC_v}{dt} - \psi_g \right) \quad (\text{eq.22})$$

$$295 \phi_{sN} = \frac{N_v}{C_v} \left(\Pi_c - \frac{dC_v}{dt} - \psi_s \right) \quad (\text{eq.23})$$

$$296 \phi_g = \begin{cases} \phi_{gP} & \phi_{gP} \times \frac{C_v}{P_p} > \phi_{gN} \times \frac{C_v}{N_v} \\ \phi_{gN} & \phi_{gN} \times \frac{C_v}{N_v} > \phi_{gP} \times \frac{C_v}{P_p} \end{cases} \quad (\text{eq.24})$$

$$\phi_s = \begin{cases} \phi_{SP} & \phi_{SP} \times \frac{C_V}{P_P} > \phi_{SN} \times \frac{C_V}{N_V} \\ \phi_{SN} & \phi_{SN} \times \frac{C_V}{N_V} > \phi_{SP} \times \frac{C_V}{P_P} \end{cases} \quad (\text{eq.25})$$

298
299
300 where $\frac{P_P}{C_V}$ is the inverse of whole plant C:P ratio, $\frac{N_V}{C_V}$ is inverse plant C:N ratio, $\frac{dC_V}{dt}$ is rate of change in plant C
301 (see Clark *et al.*, (2011) for more detail), Π_c is nutrient-unlimited, or potential, NPP (kg C m⁻² yr⁻¹), ψ_g is excess
302 C due to either P or N limitation for plant growth (kg C m⁻² yr⁻¹) and ψ_s is excess C due to either P or N
303 limitation for vegetation spreading (kg C m⁻² yr⁻¹).

304
305 Equations 20 and 22 are solved by first setting $\psi_g = 0.0$ to find the total plant P (eq. 20) and N demand (eq.22).
306 If the P and N demand for growth are less than the available P and N and fractional coverage (λ) (NPP fraction
307 used for fractional cover increment; for detail see Wiltshire *et al.*, (2021)) at the considered timestep Δt then
308 there is no limitation to growth (i. e. $\phi_{gP} < \frac{(1-\lambda)P_{avail}}{\Delta t}$; $\phi_{gN} < \frac{(1-\lambda)N_{avail}}{\Delta t}$). Where there is limited P and/or N
309 availability, the uptake equals the available P and N ($\phi_{gP} = \frac{(1-\lambda)P_{avail}}{\Delta t}$; $\phi_{gN} = \frac{(1-\lambda)N_{avail}}{\Delta t}$), and the plant
310 growth which cannot be achieved due to nutrient constraints will be deducted from potential NPP, here termed
311 excess C term (ψ_g), to give an actual NPP. Following Wiltshire *et al.*, 2021, we assume excess C is respired by
312 the plant.

313 Similarly, in order to estimate the P and N demand for spreading (eq. 21 and 23), initially the excess C from
314 spreading is set to 0.0 ($\psi_s = 0.0$), i.e under the assumption that there is no nutrient limitation. If the P and N
315 demand for spreading are lower than the available P and N and fractional coverage (λ) ($\phi_{sP} <$
316 $\frac{(1-\lambda)P_{avail}}{\Delta t}$; $\phi_{sN} < \frac{(1-\lambda)N_{avail}}{\Delta t}$), then there is no limitation on spreading and in case of limited P and N
317 availability, the uptake equals the available P and N ($\phi_{sP} = \frac{(1-\lambda)P_{avail}}{\Delta t}$; $\phi_{sN} = \frac{(1-\lambda)N_{avail}}{\Delta t}$), and the excess C
318 for spread (ψ_s) is subtracted from potential NPP.

319
320 Plant P uptake (F_p^{up}) (arrow a in Fig 1) is estimated based on the P demand for growth and spreading (ϕ_t) and
321 the root uptake capacity (u^{max}) (kg P kg⁻¹ C yr⁻¹), as follows:

$$F_p^{up} = \begin{cases} \phi_t & \phi_t \leq u^{max} \\ u^{max} & \phi_t > u^{max} \end{cases} \quad (\text{eq.26})$$

324
325 Description of the plant P uptake (F_p^{up}) varies spatially depending on the root uptake capacity (u^{max}) followed
326 by Goll *et al.*, (2017). Therefore, in regions with limited P supply, the plant P uptake is limited to the u^{max} and
327 consequently impacts the excess C and BP.

328 The root uptake capacity depends on the maximum root uptake capacity (v_{max}) (kg P kg⁻¹ C yr⁻¹), root depth
329 (d_{root}), the concentration of inorganic p at different soil depths (P_{in}), and a half saturation term at which half of
330 the maximum uptake capacity is reached using inorganic p at different soil depths (P_{in}), a scaling uptake ratio
331 (K_p) ($\mu\text{mol P l}^{-1}$), unit conversion (C_f) (1 kg P⁻¹), and soil moisture (θ) (1 m⁻²), as follows:

$$u^{max} = v_{max} \times d_{root} \times \sum_{n=1}^N P_{in_n} \times \left(\frac{1}{\sum_{n=1}^N P_{in_n} + c_f \times K_p \times \theta_n} \right) \quad (\text{eq.27})$$

334
335 Description of the litter production of P ($F_{P_n}^{lit}$) (arrow b in Fig 1) follows JULES-CN as in Wiltshire *et al.*,
336 (2021) and is calculated based on the litter flux of C (kg C m⁻² yr⁻¹) using leaf, root and wood turnovers (yr⁻¹),
337 and through the vegetation dynamics due to large-scale disturbance and litter production density, as follows:

$$F_{P_n}^{lit} = (1 - k_{leaf}) \gamma_{leaf} C_{leaf} \times C:P_{leaf} + (1 - k_{root}) \gamma_{root} C_{root} \times C:P_{root} + \gamma_{wood} C_{wood} \times C:P_{stem} \quad (\text{eq.28})$$

341
342 where λ is the leaf, root and stem re-translocation (at daily timestep) coefficient (Zachle and Friend, 2010; Clark
343 *et al.*, 2011) and the related C:P ratios for P fraction and γ is a temperature dependent turnover rate representing
344 the phenological state (Clark *et al.*, 2011).

345
346

347 The decomposition of litter (dec^{lit}) (arrow c in Fig 1) depends on soil respiration (R) ($\text{kg C m}^{-2} \text{ yr}^{-1}$), the litter
 348 C:P ratio ($C:P_{lit}$) at each soil layer (n) as follows:

$$349 \quad 350 \quad dec_p^{lit} = \frac{\sum_{n=1}^N R_n}{C:P_{lit}} \quad (\text{eq.29})$$

351 where the $C:P_{lit}$ is calculated based on litter C pool (DPM and RPM) (lit^C) ($\text{kg C m}^{-2} \text{ yr}^{-1}$) and litter P pool
 352 (P_{O_i}) as follows:

$$353 \quad 354 \quad 355 \quad C:P_{lit} = \frac{\sum_{n=1}^N lit_n^C}{P_{O_{i_n}}} \quad (\text{eq.30})$$

356 The mineralized (F_{minl_p}) (arrow d in Fig 1) and immobilized (F_{immob_p}) (arrow e in Fig 1) P fluxes are
 357 calculated based on C mineralization and immobilization, C:P ratios of plant (i) (DPM/RPM) ($C:P_{plant}$) and
 358 soil (HUM/BIO) ($C:P_{soil}$), soil pool potential respiration (R_{POT_i}) ($\text{kg C m}^{-2} \text{ yr}^{-1}$) and the respiration partitioning
 359 fraction ($resp_frac$) as follows:

$$360 \quad 361 \quad 362 \quad F_{minl_{p_n}} = \frac{\sum_{n=1}^N R_{POT_{i_n}}}{\epsilon_{cp_i}} \quad (\text{eq.31})$$

$$363 \quad 364 \quad F_{immob_{p_n}} = \frac{\sum_{n=1}^N R_{i_n} \times resp_frac}{C:P_{soil}} \quad (\text{eq.32})$$

365 The soil respiration from each soil layer ($R_{i,n}$) is estimated from potential soil respiration ($R_{POT_{i,n}}$) for the
 366 DPM, RPM pools and the litter decomposition rate modifier (F_{P_n}) as follows:

$$367 \quad 368 \quad 369 \quad R_{i,n} = R_{POT_{i,n}} \times F_{P_n} \quad (\text{eq.33})$$

370 where the description of F_{P_n} for P pools ($F_{P_{P_n}}$) follows Wang *et al.* (2007) and is estimated based on the soil
 371 pool (BIO/HUM) mineralization ($minl_{p-BIO_n}$, $minl_{p-HUM_n}$) and immobilization ($immob_{p-BIO_n}$,
 372 $immob_{p-HUM_n}$) (in $\text{kg P m}^{-2} \text{ yr}^{-1}$), soil inorganic P (P_{inorg_n}) (in kg P m^{-2}), and litter pools (DPM/RPM) demand
 373 (in $\text{kg P m}^{-2} \text{ yr}^{-1}$) as follows:

$$374 \quad 375 \quad 376 \quad F_{P_{P_n}} = \frac{(minl_{p-BIO_n} + minl_{p-HUM_n} - immob_{p-BIO_n} - immob_{p-HUM_n}) + P_{inorg_n}}{DEM_{DPM_n} + DEM_{RPM_n}} \quad (\text{eq.34})$$

377 The net demand associated with decomposition of litter pools ($DEM_{k,n}$) represents the P required by microbes
 378 which convert DPM and RPM into BIO and HUM. The limitation due to insufficient P availability is estimated
 379 based on the potential mineralization ($minl_{p-pot}$) and immobilization ($immob_{p-pot}$) (in $\text{kg P m}^{-2} \text{ yr}^{-1}$) of pools
 380 (k) as follows:

$$381 \quad 382 \quad 383 \quad DEM_{k,n} = immob_{p-pot,k} - minl_{p-pot,k} \quad (\text{eq.35})$$

384 The F_{P_n} estimated for N pools ($F_{P_{N_n}}$) follows the same formulation as P (see Wiltshire *et al.*, 2021 for detail)
 385 and the F_{P_n} is estimated based on a higher rate modifier between N and P as follows:

$$386 \quad 387 \quad 388 \quad F_{P_n} = \begin{cases} F_{P_{P_n}} & F_{P_{P_n}} > F_{P_{N_n}} \\ F_{P_{N_n}} & F_{P_{N_n}} > F_{P_{P_n}} \end{cases} \quad (\text{eq.36})$$

389 Description of the fluxes of adsorption ($F_{P_{in_n}^{sorp}}$) (arrow e in Fig 1) and desorption ($F_{P_{in_n}^{desorp}}$) (arrow f in Fig
 390 1) of inorganic P in $\text{kg P m}^{-2} \text{ yr}^{-1}$ follow Wang *et al.*, (2010) and are calculated based on soil inorganic (P_{in_n}) and
 391 sorbed inorganic ($P_{inorg-sorbed_n}$) P pools and inorganic adsorption ($K_{sorp-in}$), desorption ($K_{desorp-in}$)
 392 coefficients ($\text{kg P m}^{-2} \text{ yr}^{-1}$) and maximum sorbed inorganic (P_{in-max}) (kg P m^{-2}) as follows:

$$393 \quad 394 \quad 395 \quad F_{P_{in_n}^{sorp}} = P_{in_n} \times K_{sorp-in} \times \frac{(P_{in-max_n} - P_{inorg-sorbed_n})}{P_{in-max_n}} \quad (\text{eq.37})$$

396

$$F_{P_{in_n}}^{desorp} = P_{inorg-sorbed_n} \times K_{desorp-in} \quad (\text{eq.38})$$

398

399 [Description of the occluded inorganic P flux \(\$F_{P_n}^{occ}\$ \) \(arrow g in Fig 1\) follows Wang *et al.*, \(2007\) and Hou *et al.*, \(2019\) and](#) is calculated based on sorbed inorganic P pool and P occlusion rate (K_{occ}) (kg P m⁻² yr⁻¹) as follows:

402

$$F_{P_n}^{occ} = P_{inorg-sorbed_n} \times K_{occ} \quad (\text{eq.39})$$

404

405 [Description of the fluxes of adsorption \(\$F_{P_{O_{S_n}}}^{sorp}\$ \) \(arrow h in Fig 1\) and desorption \(\$F_{P_{O_{S_n}}}^{desorp}\$ \) \(arrow i in Fig 1\) of organic P follow Wang *et al.*, \(2010\) are calculated based on soil organic and sorbed organic P pools and organic adsorption \(\$K_{sorp-or}\$ \) \(kg P m⁻² yr⁻¹\), desorption \(\$K_{desorp-or}\$ \) coefficients \(kg P m⁻² yr⁻¹\) and maximum sorbed organic \(\$P_{org-max}\$ \) \(which corresponds to the sorbed soil P saturation, thus modifying the sorption rate respectively\) \(kg P m⁻²\) as follows:](#)

410

$$F_{P_{O_{S_n}}}^{sorp} = P_{O_{S_n}} \times K_{sorp-or} \times \frac{(P_{or-max_n} - P_{org-sorbed_n})}{P_{or-max_n}} \quad (\text{eq.40})$$

412

$$F_{P_{O_{S_n}}}^{desorp} = P_{org-sorbed_n} \times K_{desorp-or} \quad (\text{eq.41})$$

414

415 [Description of the occluded organic P flux \(\$F_{P_n}^{or-occ}\$ \) \(kg P m⁻² yr⁻¹\) \(arrow j in Fig 1\) follows Wang *et al.*, \(2007\) and Hou *et al.*, \(2019\) is calculated based on sorbed organic P pool \(\$P_{org-sorbed_n}\$ \) and P occlude rate \(\$K_{occ}\$ \) \(kg P m⁻² yr⁻¹\) as follows:](#)

418

$$F_{P_n}^{or-occ} = P_{org-sorbed_n} \times K_{occ} \quad (\text{eq.42})$$

420

421 [Description of the P flux from weathered parent material \(\$F_{P_n}^w\$ \) \(arrow k in Fig 1\) follows Wang *et al.*, \(2007\) and](#) is calculated based on amount of P in the parent material (P_{pm}) and P weathering rate (K_w) (kg P m⁻² yr⁻¹) as follows:

424

$$F_{P_n}^w = P_{pm_n} \times K_w \quad (\text{eq.43})$$

426

427 [Description of P diffusion between soil layers \(\$F_{D_n}\$ \) expressed in \(kg P m⁻² yr⁻¹\) \(arrow l in Fig 1\) follows Goll *et al.*, \(2017\) and](#) is calculated following Fick's second law and it is a function of the diffusion coefficient (Dz) in m² s⁻¹, the concentration of inorganic P at different soil depths (P_{in}) in kg P m⁻², the distance (z) between the midpoints of soil layers in metres and seconds to year unit conversion (Yr):

431

$$F_{D_n} = \frac{\partial}{\partial z} (D_{z_n} \frac{\partial P_{S_n}}{\partial z}) \times Yr \quad (\text{eq.44})$$

433

434

435

436

437

438

439

440

441

442

443

444

445

446

447

448 **Table 1.** Model variables

Variable	Unit	Definition
Ψ	kg C m ⁻² yr ⁻¹	Excess C flux
\emptyset	kg P m ⁻² yr ⁻¹	Plant demand for uptake
Π_c	kg C m ⁻² yr ⁻¹	Potential NPP
u^{max}	kg P kg ⁻¹ C yr ⁻¹	Root uptake capacity
DEM	kg P m ⁻² yr ⁻¹	Plant pool P associated decomposition demand
dec_P^{lit}	kg P m ⁻² yr ⁻¹	Litter decomposition
F_D	kg P m ⁻² yr ⁻¹	Plant diffusion flux
F_P	-	Plant litter decomposition rate modifier
F_P^{lit}	kg P m ⁻² yr ⁻¹	Plant litter flux
F_P^{up}	kg P m ⁻² yr ⁻¹	Plant uptake
$F_{PO_S}^{sorp}$	kg P m ⁻² yr ⁻¹	Sorbed organic P flux
$F_{P_{in}}^{sorp}$	kg P m ⁻² yr ⁻¹	Sorbed inorganic P flux
$F_{PO_S}^{desorp}$	kg P m ⁻² yr ⁻¹	Desorbed organic P flux
$F_{P_{in}}^{desorp}$	kg P m ⁻² yr ⁻¹	Desorbed inorganic P flux
F_P^{occ}	kg P m ⁻² yr ⁻¹	Occluded inorganic P flux
F_P^{or-occ}	kg P m ⁻² yr ⁻¹	Occluded organic P flux
F_P^w	kg P m ⁻² yr ⁻¹	Weathered P flux
F_{immob_P}	kg P m ⁻² yr ⁻¹	Immobilized P flux
lit_C	kg C m ⁻² yr ⁻¹	C litter flux
lit_{frac}	-	Litter fraction
lit_{leaf}	kg C m ⁻² yr ⁻¹	Leaf litter flux
lit_{root}	kg C m ⁻² yr ⁻¹	Root litter flux
lit_{wood}	kg C m ⁻² yr ⁻¹	Woody litter flux
F_{minl_P}	kg P m ⁻² yr ⁻¹	Mineralized P flux
P_p	kg P m ⁻²	Plant P pool
P_{O_l}	kg P m ⁻²	Litter organic pool
P_{O_s}	kg P m ⁻²	Soil organic pool
P_{in}	kg P m ⁻²	Soil inorganic pool
$P_{inorg-sorp}$	kg P m ⁻²	Soil inorganic sorbed pool
$P_{org-sorp}$	kg P m ⁻²	Soil organic sorbed pool
P_{occ}	kg P m ⁻²	Soil occluded pool
P_{pm}	kg P m ⁻²	Parent material pool
R	kg C m ⁻² yr ⁻¹	Total respiration
R_{POT}	kg C m ⁻² yr ⁻¹	Total potential respiration
R^s	kg C m ⁻² yr ⁻¹	Soil respiration
R_d	kg C m ⁻² yr ⁻¹	Leaf dark respiration
T_{ref}	K	Soil reference temperature
T_s	K	Soil temperature
Veg_c	kg C m ⁻²	Sum of biomass
z	m	Soil depth

449

450

451

452

453

454

455
456

Table 2. P Model parameters

Parameter	Value	Unit	Eq.	Description	Source
C and N related					
α	0.25	-	6	Plant type material ratio	(Clark <i>et al.</i> , 2011)
a_{wl}	1.204	kg C m ⁻²	50	Allometric coefficient	calibrated
σ_l	0.0375	kg C m ⁻² per unit LAI	48	Specific leaf density	Clark <i>et al.</i> , 2011
b_{wl}	1.667	-	50	Allometric exponent.	Clark <i>et al.</i> , 2011
f_{dr}	0.005	-	47	Respiration scale factor	Calibrated
$resp_frac$	0.25	-	32	Respiration fraction	(Clark <i>et al.</i> , 2011)
k_{leaf}	0.5	-	28	Leaf N re-translocation coefficient	(Zachle and Friend, 2010)
k_{root}	0.2	-	28	Root N re-translocation coefficient	(Zachle and Friend, 2010)
d_{root}	3.0	-	27	Root fraction in each soil layer	(Clark <i>et al.</i> , 2011)
v_{int}	7.21	μmol CO ₂ m ⁻² s ⁻¹	45	Intercept in the linear regression between V_{cmax} and N_{area}	Calibrated (Clark <i>et al.</i> , 2011)
v_{sl}	19.22	μmol CO ₂ gN ⁻¹ s ⁻¹	45	Slope in the linear regression between V_{cmax} and N_{area}	Calibrated (Clark <i>et al.</i> , 2011)
LMA	131.571852	g m ⁻²	45	Observed Leaf Mass per Area	Study site
$Leaf\ N$	1.79007596	g g ⁻¹	45, 46	Foliar N concentrations in area basis	Study site
P related					
$C:P_{soil}$	1299.6	-	32	Soil C:P ratio	(Fleischer <i>et al.</i> , 2019)
v_{max}	0.0007	kg P kg ⁻¹ C yr ⁻¹	27	Maximum root uptake capacity	Calibrated (Goll <i>et al.</i> , 2017)
P	0.7083062	g kg ⁻¹	46	Foliar P concentrations	Study site
c_f	3.1×10 ⁻⁵	l kg P ⁻¹	27	Conversion factor	(Goll <i>et al.</i> , 2017)
D_z	0.001	m ² s ⁻¹	44	Diffusion coefficient	(Burke <i>et al.</i> , 2017)
K_{occ}	1.2×10 ⁻⁵	yr ⁻¹	39, 42	P occlusion rate	(Yang <i>et al.</i> , 2014)
K_p	3.0	kg P l ⁻¹	27	Scaling uptake ratio	Calibrated
$K_{sorp-in}$	0.0054	kg P m ⁻² yr ⁻¹	37	Inorganic P adsorption coefficient	Calibrated (Hou <i>et al.</i> , 2019)
$K_{sorp-or}$	0.00054	kg P m ⁻² yr ⁻¹	40	Organic P adsorption coefficient	Calibrated
K_{in-max}	0.0075	kg P m ⁻² yr ⁻¹	37	Maximum sorbed inorganic P	Study site
K_{or-max}	0.0042	kg P m ⁻² yr ⁻¹	40	Maximum sorbed organic P	Study site
K_w	3×10 ⁻⁶	kg P m ⁻² yr ⁻¹	43	P weathering rate	(Wang <i>et al.</i> , 2010)

457
458
459

2.3 Study sites

460 This study uses data from two nearby sites in Central Amazon in Manaus, Brazil. The main site from here on
461 termed *study site* (2°35'21.08" S, 60°06'53.63" W) (Lugli *et al.*, 2020) is for model development and
462 evaluation. The second site is the Manaus K34 flux site (2°36'32.67" S, 60°12'33.48" W) which provides
463 meteorological station data for running the model but also provides data for model evaluation. Our study site is
464 the main lowland tropical forest site maintained by the National Institute for Amazon Research (INPA).
465 Research at this site focuses on pre-experimental, plot, and full-scale long-term projects, combining
466 experimental approaches (Keller *et al.*, 2004; Malhi *et al.*, 2009) with modelling (Lapola and Norby, 2014).
467 Moreover, a recent manipulation experiment at this site provides an opportunity for future model testing under P
468 fertilization. We use detailed novel soil and plant P pool data from the *study site* (Lugli *et al.*, 2020, 2021) for
469 model parameterisation and calibration and carbon stock data for model validation. The *study site* has a very
470 similar forest, geomorphology, soil chemistry and species composition to the well-known and studied K34 eddy
471 covariance flux site (Araújo *et al.*, 2002). The average reported annual precipitation is 2431 (mm yr⁻¹), with a
472 monthly range of 95 to 304 (mm month⁻¹), and averaged temperature is 26°C (Araújo *et al.*, 2002). Moreover,
473 the soil class at this site is Geric Ferrosol with a high clay content and weathering activities (Malhi *et al.*, 2004).

474
475
476

2.4 Model parameterisation, calibration and evaluation

477 We use observations from the four control plots of the [study site](#) to parameterise, calibrate and evaluate different
478 processes in JULES (Table 3). The observations were collected at 4 soil depths and processed using the Hedley
479 sequential fractionation (Hedley, Stewart and Chauhan, 1982; Quesada *et al.*, 2010). Observed Leaf Mass per
480 Area (LMA) leaf N and leaf P estimated from fresh leaves were used as input parameters to JULES to estimate
481 photosynthetic capacity and respiration parameters. JULES vn5.5 ([JULES CN in this study](#)) estimates V_{cmax}
482 ($\mu\text{mol m}^{-2} \text{s}^{-2}$) based on Kattge *et al.* (2009) using [foliar N concentrations in area basis \(\$n_{leaf}\$ \)](#), as follows:
483

$$484 \quad V_{cmax} = v_{int} + v_{sl} * n_{leaf} \quad (\text{eq.45})$$

485
486 where v_{int} is the estimated intercept and v_{sl} is the slope of the linear regression derived for the V_{cmax} estimation.
487 We incorporated an additional P dependency on the estimation of V_{cmax} following Walker *et al.* (2014) as
488 follows:
489

$$490 \quad \ln(V_{cmax}) = 3.946 + 0.921 \ln(N) + 0.121 \ln(P) + 0.282 \ln(N) \ln(P) \quad (\text{eq.46})$$

491
492 Where N and P are foliar concentrations in area basis.
493

494 Implementation of eq. 46 resulted in higher V_{cmax} than in the original version of JULES. A higher V_{cmax} predicted
495 higher leaf and plant respiration (eq.47). Constrained by observations of NPP and plant respiration at the study
496 site, we modified one of the most uncertain parameters in the description of plant respiration (f_{dr}) (eq.47) which
497 is the scale factor (f_{dr}) for leaf dark respiration (R_d) as follows:
498

$$499 \quad R_d = f_{dr} V_{cmax} \quad (\text{eq.47})$$

500
501 The default value for this scale factor is 0.01 (Clark *et al.*, 2011), and for JULES-CNP simulations at our study
502 site it was modified to 0.005.

503 Observations of aboveground biomass were used to calibrate the non PFT dependent allometric relationships in
504 JULES (Clark *et al.* 2011) (eq 48-50) for leaf, root and stem C. Specifically, the a_{wl} parameter (eq 50) was
505 modified from 0.65 to 1.204 to match better tropical forest allometry:
506

$$507 \quad C_{leaf} = \sigma_l L_b \quad (\text{eq.48})$$

$$508 \quad C_{root} = C_{leaf} \quad \text{_(eq.49)}$$

$$509 \quad C_{stem} = a_{wl} L_b^{b_{wl}} \quad \text{_(eq.50)}$$

510
511 Where σ_l is specific leaf density (kg C m^{-2} per unit LAI), L_b is balanced (or seasonal maximum) leaf area index
512 ($\text{m}^2 \text{m}^{-2}$), a_{wl} is allometric coefficient (kg C m^{-2}) and b_{wl} is allometric exponent.

513 [Note that JULES CNP uses C3 and C4 photosynthesis model from Collatz *et al.*, 1991; Collatz, Ribas-Carbo
514 and Berry, 1992, which does not include estimation of \$J_{max}\$.](#)

515 [JULES-CNP has fixed stoichiometry and C:P ratios of leaf and root \(measured\), and wood \(estimated from
516 fresh coarse wood \(Lugli, 2013\)\) which were taken from the *study site* and prescribed in JULES to simulate P
517 dynamics in the plant.](#) The following belowground data were used to represent various soil P pools: Resin and
518 bicarbonate inorganic P (inorganic P: P_{in}), organic bicarbonate P (organic P: P_{OS}), NaOH organic P (sorbed
519 organic P: $P_{org-sorp}$), NaOH inorganic P (sorbed inorganic P: $P_{inorg-sorp}$), residual P (occluded P: P_{occ}) and
520 HCL P (parent material P: P_{pm}) (Table 3). [The measurements were collected between 2017 and 2018 in control
521 plots. All measurements were conducted at four soil layers \(0-5 ,5-10, 10-20, 20-30 cm\). However, to be
522 consistent with the JULES model soil layer discretization scheme, we defined 4 soil layers \(0-10 cm, 10-30 cm,
523 30-100 cm and 100-300 cm\) and we used the average between 0 and 30 cm to compare against the measurement
524 from the same depth for model evaluation.](#)

525 [Vegetation C stocks were derived based on tree diameter measurements at breast height, that are linked to
526 allometric equations and wood density databases to estimate the C stored in each individual tree, and then scaled
527 to the plot \(Chave *et al.*, 2014\).](#)

528
529 [The organic and inorganic soil P assumed to be always at equilibrium with the relative sorbed pools](#) (Wang,
530 Law and Pak, 2010). [Thus, in](#) order to cap P sorption and uptake capacity, the maximum sorption capacities
531 (P_{in-max_n} , P_{or-max_n} , eq.37 and 39) [\(adopted from](#) (Wang, Houlton and Field, 2007)) [were prescribed using](#)
532 [maximum](#) observed sorbed inorganic and organic P. Hence, the maximum sorption capacity defines the

equilibrium state of sorbed and free-soil P. [Moreover, as the magnitude of changes in the occluded and parent material pools are insignificant over a short-term \(20 years\) simulation period \(Vitousek *et al.*, 1997\), these two pools were prescribed using observations.](#) Remaining parameters used to describe soil P fluxes (eq.s [27-44](#)) were prescribed using values from the literature (Table 3).

[We used a combination of data from *Study site* and the nearby site K34 for model evaluation of C fluxes \(GPP, NPP\) and C pools \(soil and vegetation C, leaf, root and stem C\) with no calibration on plant and soil organic and soil inorganic P pools included \(Table 3\).](#)

Table 3. Observations from [study site](#) (taken during 2017-2018) and from Manaus site K34 used for model parameterisation and evaluation

Process	Variables	Purpose of use	Reference and site
C associated	GPP	Evaluation	Fleischer <i>et al.</i> , 2019, K34
	NPP	Evaluation	Fleischer <i>et al.</i> , 2019, K34
	Soil C	Evaluation	Malhi <i>et al.</i> , 2009, K34
	CUE	Evaluation	Malhi <i>et al.</i> , 2009, K34
	Veg C	Evaluation	Study site
	Leaf C	Evaluation	Study site
	Stem C	Evaluation	Study site
	Root C	Evaluation	Study site
	LAI	Initialisation	Study site
	LMA	Parameterisation	Study site
P associated	Resin	Evaluation	Study site
	Pi Bic	Evaluation	Study site
	Po Bic	Evaluation	Study site
	Po NaOH	Calibration	Study site
	Pi NaOH	Calibration	Study site
	P residual	Parameterisation	Study site
	P HCL	Parameterisation	Study site
	Leaf N	Parameterisation	Study site
	Leaf P	Parameterisation	Study site
	Root P	Parameterisation	Study site
Plant C:P ratio	Parameterisation	Study site	

2.5 JULES simulations

JULES was applied at the K34 flux tower site using observed meteorological forcing data from 1999-2019 (Fleischer *et al.* 2019) at half hourly resolution. [The following meteorological variables are needed to drive JULES \(model inputs\)](#) (Best *et al.*, 2011): atmospheric specific humidity (kg kg^{-1}), atmospheric temperature (K), air pressure at the surface (Pa), short and longwave radiation at the surface (W m^{-2}), wind speed (m s^{-1}) and total precipitation ($\text{kg m}^{-2} \text{s}^{-1}$). [Furthermore, the averaged measured LAI from study site was used to initialise the vegetation phenology module, but was allowed to vary in subsequent prognostic calculations.](#) [Soil organic and inorganic sorbed P pools were initialised with study site observations.](#) [The JULES CNP simulations were initialized following the same methodology as in Fleischer *et al.*, \(2019\), by the spin-up from 1850 recycling climatology to reach equilibrium state \(Figure S1\) and spin up was performed separately for three versions of JULES \(C/CN/CNP\) following the same procedure.](#) [Furthermore, the transient run was performed for the period 1851-1998 using time-varying \$\text{CO}_2\$ and N deposition fields. Finally, for the extended simulation period \(1999-2019\) two runs were performed, the first with ambient the second elevated \$\text{CO}_2\$ concentrations.](#)

We evaluate the impact of including a P cycle in JULES using three model configurations (JULES C, CN and CNP). We apply JULES in all three configurations using present day climate under both ambient CO_2 and elevated CO_2 (e CO_2). Ambient and e CO_2 were prescribed following Fleischer *et al.*, (2019), [with present-day \$\text{CO}_2\$ based on global monitoring stations, and an abrupt \(step\) increase in atmospheric \$\text{CO}_2\$ of +200 ppm on the onset of the transient period \(i.e., 1999\).](#) However, the comparison period is limited to 2017-18 for which the P measurements are available.

We compare simulated C fluxes (GPP, NPP, litterfall C), C stocks (total vegetation, fine root, leaf, wood, soil) and the CO_2 fertilization effect across model configurations. The CO_2 fertilization effect ($\text{CO}_{2\text{fert-eff}}$) (eq. [51](#)) is calculated based on simulated vegetation C under ambient ($\text{VegC}(\text{aCO}_2)$) and e CO_2 ($\text{VegC}(\text{eCO}_2)$) as follows:

570

$$CO2_{fert-eff} = \frac{(VegC(eCO_2) - VegC(aCO_2)) \times 100}{VegC(aCO_2)} \quad (\text{eq.51})$$

572

573 Furthermore, the net biomass increases due to CO₂ fertilization effect (ΔC_{veg}) is estimated as follows:

574

$$\Delta C_{veg} = \Delta BP - \Delta litterfall C \quad (\text{eq.52})$$

576

577 [We studied the Water Use Efficiency \(WUE\) \(eq. 53\) at half-hourly timestep, then aggregated per month](#) as one
578 of the main indicators of GPP changes (Xiao *et al.*, 2013), and soil moisture [content](#) (SMCL), as one of the
579 main controllers of maximum uptake capacity (eq. 27), in order to better understanding the changes in GPP, P
580 demand and uptake as well as [excess C](#) fluxes.

581

$$WUE = GPP / Transpiration \quad (\text{eq.53})$$

583

584 Moreover, we also estimated the Carbon Use Efficiency (CUE) as an indicator of the required C for the growth
585 (Bradford and Crowther, 2013) as follows:

586

$$CUE = BP / GPP \quad (\text{eq.54})$$

588

589 [We use JULES-CNP to evaluate the extent of P limitation under ambient and eCO₂ at this rainforest site in](#)
590 [Central Amazon. P limitation is represented by the amount of C that is not used to grow new plant tissue due to](#)
591 [insufficient P in the system \(excess C\) \(eq. 27\). The excess C flux is highly dependent on the plant P and the](#)
592 [overall P availability to satisfy demand. We also explore the distribution of the inorganic and organic soil P and](#)
593 [their sorbed fraction within the soil layer and under ambient and eCO₂.](#)

594

595 [To test the sensitivity of the P and C related processes to the model P parameters, six sets of simulations were](#)
596 [conducted with modified plant C:P stoichiometry \(Plant C:P: *SENS1*\), P uptake scaling factor \(K_P\) \(K_P: *SENS2*\),](#)
597 [inorganic \(K_{P_sorb_in}: *SENS3*\) and organic \(K_{P_sorb_or}: *SENS4*\) P adsorption coefficients](#)
598 [\(K_{sorb-or}, K_{sorb-in}\), and maximum inorganic \(K_{P_sorb_in_max}: *SENS5*\) and organic \(K_{P_sorb_or_max}:](#)
599 [SENS6\) sorbed P \(K_{or-max}, K_{in-max}\). These values were prescribed to vary between ±50% of the observed](#)
600 [values and their effect on C pools \(plant and soil C\) and fluxes \(NPP and excess C\), and P pools \(plant, soil, and](#)
601 [soil sorbed P\) was assessed. As the derived model parameters from measurements have their own level of](#)
602 [uncertainty, we took the 50% of the change to test these parameters at reasonable degree. However, the](#)
603 [occluded and weathered P pools are prescribed for this model application, the occluded and weather P](#)
604 [coefficients \(other two P-related model parameters\) were not part of sensitivity tests.](#)

605

606 Our model evaluation period is limited to years 2017-18 due to the P measurement availability. However, in
607 order to perform inter-models comparison with 15 models studied by Fleischer *et al.*, (2019) we also studied the
608 response of GPP, NPP and BP to eCO₂ for both initial (1999) and 15 years periods (between 1999-2013).

609

610

611

612

613

614

615

616

617

618

619

620

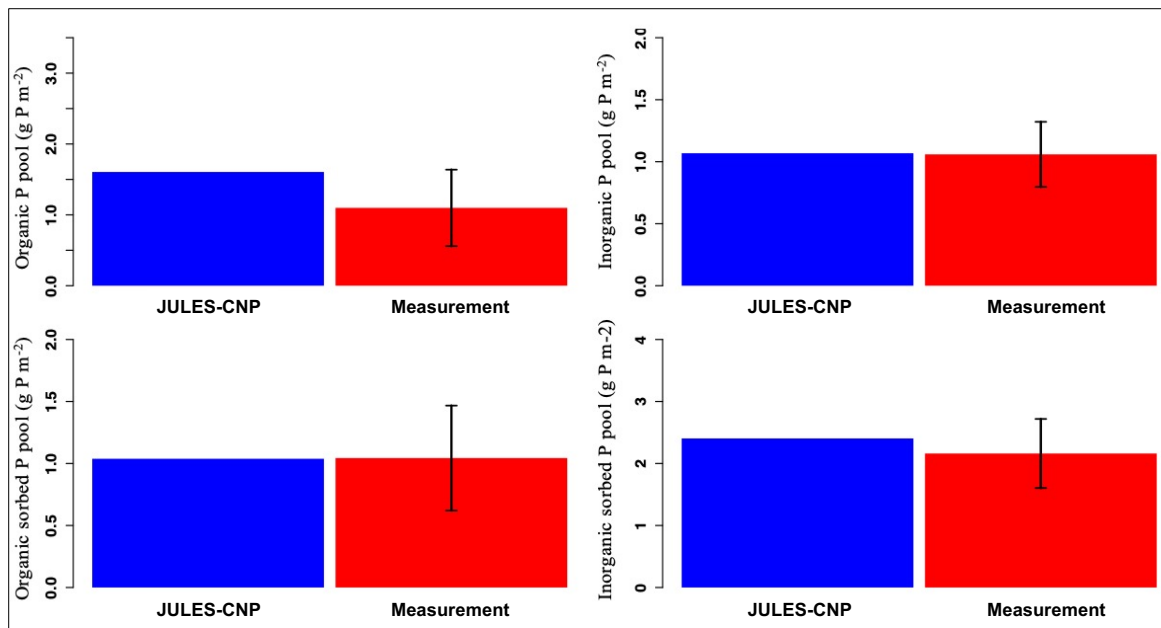
621

3. Results

3.1 Model application under ambient CO₂

3.1.1 Calibration of simulated soil P pools

The maximum sorption capacities (P_{in-max_n} , P_{or-max_n} , eq.37 and 40) were calibrated to the observed P pools. As a result, JULES-CNP could reproduce the measured soil p pools (Figure. 2 and Table 4). Simulated inorganic soil P and sorbed organic and inorganic soil P closely matched the observations (Table 5 and Figure. 2). However, simulated organic soil P overestimates the observations by 60 %.



622
623
624
625
626
627
628
Figure 2- Modelled vs measured soil phosphorus pools under ambient CO₂ (for the soil depth of 0-30cm). Black line represents standard deviation

Table 4. Observed and simulated phosphorus pools and fluxes. Occluded and weathered P pools were prescribed using the observed values (between period 2017-18).

	Phosphorus pools and fluxes		
	Measured	Modelled Ambient CO ₂	Modelled Elevated CO ₂
Organic P (g P m ⁻²)	1.09±0.53	1.6	1.57
Inorganic P (g P m ⁻²)	1.05±0.33	1.07	0.96
Sorbed organic P (g P m ⁻²)	1.04±0.42	1.04	1.03
Sorbed inorganic P (g P m ⁻²)	2.1±0.55	2.4	2.4
Occluded P (g P m ⁻²)	7.98±2.38	prescribed	prescribed
Weathered P (g P m ⁻²)	0.59±12	prescribed	prescribed
Total vegetation P (g P m ⁻²)	4.15	4.66	5.11
Soil P – 30cm (g P m ⁻²)	13.85	14.7	14.56
Total ecosystem P (g P m ⁻²)	-	35.97	35.97
P litter flux (g P m ⁻² yr ⁻¹)	0.3	0.28	0.29

629
630
631
632
3.1.2 Model evaluation

633 [JULES CNP-CNP could reproduce the plant and soil C \(Figure.2 and Table 5\) and N pools and fluxes \(Figure](#)
634 [S6 and Table 6\) pools and fluxes under ambient CO₂](#). Our results show that simulated GPP, is within the range
635 of measurement (3.02 kg C m⁻² yr⁻¹ model vs 3-3.5 kg C m⁻² yr⁻¹ observed, respectively, Table 5).
636

637 Simulated NPP, is close to the measured values (NPP: 1.14 - 1.31 observed vs 1.26 modelled kg C m⁻² yr⁻¹) with
638 autotrophic respiration (RESP) also closely following the observations (1.98 observed vs 1.81 modelled kg C m⁻²
639 yr⁻¹). Biomass production is estimated as a difference between NPP and the amount of C which is not fixed by
640 plants due to the insufficient P in the system ([excess C](#)) (eq. 27). The [excess C](#) flux is highly dependent on the
641 plant P and the overall P availability to satisfy demand (Table 5). Simulated flux of [excess C](#) is 0.3 kg C m⁻² yr⁻¹
642 under ambient CO₂. In JULES-CNP this flux is subtracted from NPP in order to give the BP (eq. 17) (Table 5).
643 Our simulated litterfall overestimates the observations by 32%, however simulated vegetation and its
644 components (fine root, leaf and wood) and soil C stocks match well the observations (Table 5).

645 **Table 5.** Observed and simulated carbon pools and fluxes with JULES CNP (between period 2017-18)

Carbon pools and fluxes			
	Measured	Modelled Ambient CO₂	Modelled Elevated CO₂
GPP (kg C m ⁻² yr ⁻¹)	3.0 – 3.5	3.06	3.9
NPP_{pot} (kg C m ⁻² yr ⁻¹)	-	1.27	1.77
Plant respiration (kg C m ⁻² yr ⁻¹)	1.98	1.78	2.12
Excess C flux (kg C m ⁻² yr ⁻¹)	-	0.30	0.81
Biomass Production (kg C m ⁻² yr ⁻¹)	<u>1.14±0.12</u>	0.96	0.94
Litter C flux (kg C m ⁻² yr ⁻¹)	<u>0.69±0.15</u>	0.91	0.83
Leaf C (kg C m ⁻²)	<u>0.37±0.2</u>	0.38	0.40
Wood C (kg C m ⁻²)	22.01	22.4	24.71
Root C (kg C m ⁻²)	<u>0.37±0.2</u>	0.38	0.40
Vegetation C (kg C m ⁻²)	<u>22.75±0.3</u>	23.16	25.52
Soil C stock (kg C m ⁻²)	12.7	13.2	12.71
LAI (m ² m ⁻²)	<u>5.6±0.36</u>	5.77	6.12

646

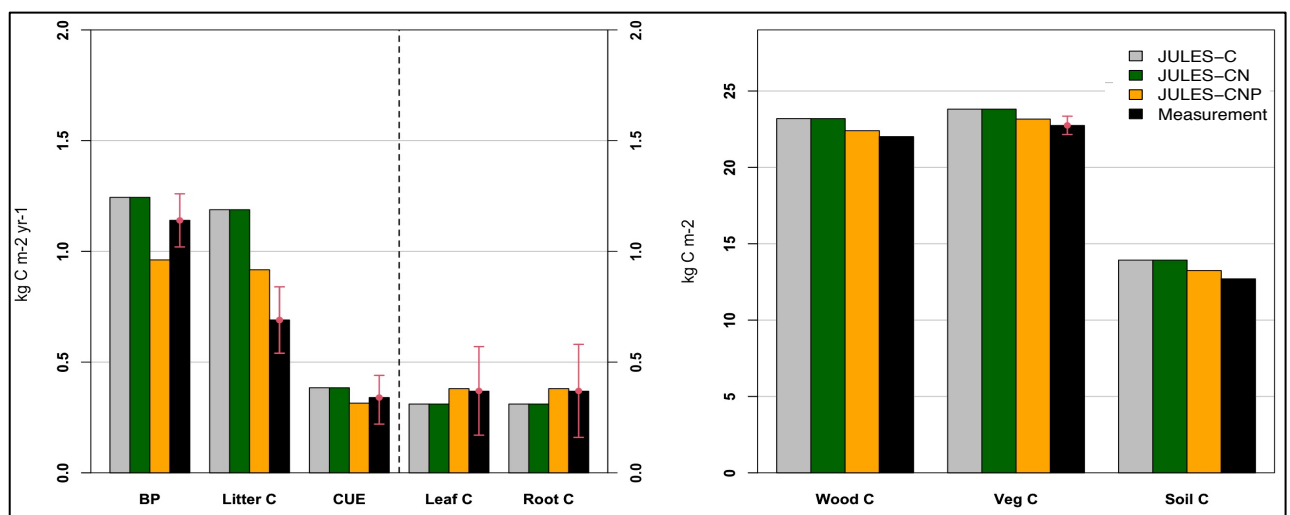
647 **3.1.3 Comparison of JULES C, CN and CNP under ambient CO₂**

648

649 We compare simulated C pools and fluxes from JULES-C, JULES-CN and JULES-CNP (Figure. 3). There is no
 650 difference between C stocks and fluxes in simulations from JULES C and CN indicating that there is no N
 651 limitation at this tropical site in the CN simulations. However, simulated BP and litter flux of C by JULES
 652 C/CN are higher than in JULES-CNP but also overestimate the observations (litter flux of JULES C/CN: 1.18,
 653 JULES CNP: 0.91 and obs 0.69 (kg C m⁻² yr⁻¹) and BP of JULES C/CN: 1.24, JULES CNP: 0.96 and obs 1.14-
 654 1.31 (kg C m⁻² yr⁻¹), respectively). By including the P cycling in JULES an **excess C** flux of 0.3 (kg C m⁻² yr⁻¹)
 655 is simulated, indicating a 24% P limitation to BP at this site according to JULES CNP, which represents a 29%
 656 decrease in BP compared to JULES-C/CN. Consequently, the total vegetation C stock for models without P
 657 inclusion is higher than the CNP version (+3% difference) due to the lack of representation of P limitation. The
 658 simulated soil C stock in JULES C and JULES CN is also higher than in the CNP version (JULES C/CN: 13.93
 659 vs. JULES CNP: 13.18 (kg C m⁻² yr⁻¹)) and higher than the observations. Moreover, CUE in JULES C/CN
 660 (eq.54) is higher than observations and JULES CNP version (JULES C/CN: 0.38 vs. JULES CNP: 0.31, obs:
 661 0.34 ±0.1(dimensionless).
 662
 663

662

663



664

665 **Figure. 3-** JULES C, CN, CNP modelled vs measured C pools (Leaf, root, wood, Veg and Soil C) (in kg C m⁻²)
 666 and fluxes (BP and Litter C) (in kg C m⁻² yr⁻¹) and CUE under ambient CO₂. Note that CUE is unitless.

667

668

669

3.1.4 Model sensitivity

The results indicate that among all the corresponding C and P pools and fluxes, the excess C flux – which demonstrates P limitation to growth – shows the highest sensitivity to changes in C:P ratios, K_P and K_{or-max} , K_{in-max} . A decrease in plant C:P results in a large increase in excess C. This is due to the higher plant P demand as a result of lower plant C:P ratios. An increase in the uptake factor and maximum sorbed organic and inorganic P also results in an increase in excess C. This is due to the higher uptake demand through higher uptake capacity (due to higher K_P) and lower available P for uptake due to higher organic and inorganic sorbed P (due to higher K_{or-max} , K_{in-max}). Since the total P in the system is lower than the plant demand, the uptake capacity and sorbed P, higher P limitation is placed on growth (decreasing BP) which results in an increase in excess C and decrease in plant C, but also soil C which is a result of lower litter input (Figure 4). Total soil P shows low sensitivity to changes in plant C:P and uptake factor but high sensitivity to maximum inorganic sorbed P. Moreover, sorbed P shows middle to high sensitivity to maximum organic and inorganic sorbed P respectively (Figure. S5). Nevertheless, organic and inorganic P adsorption coefficients ($K_{sorp-or}$, $K_{sorp-in}$) show no sensitivity to C and P pools and fluxes. This is due to limiting the organic and inorganic P sorption terms controlled only by maximum sorption, hence no effect applied by organic and inorganic adsorption coefficients.

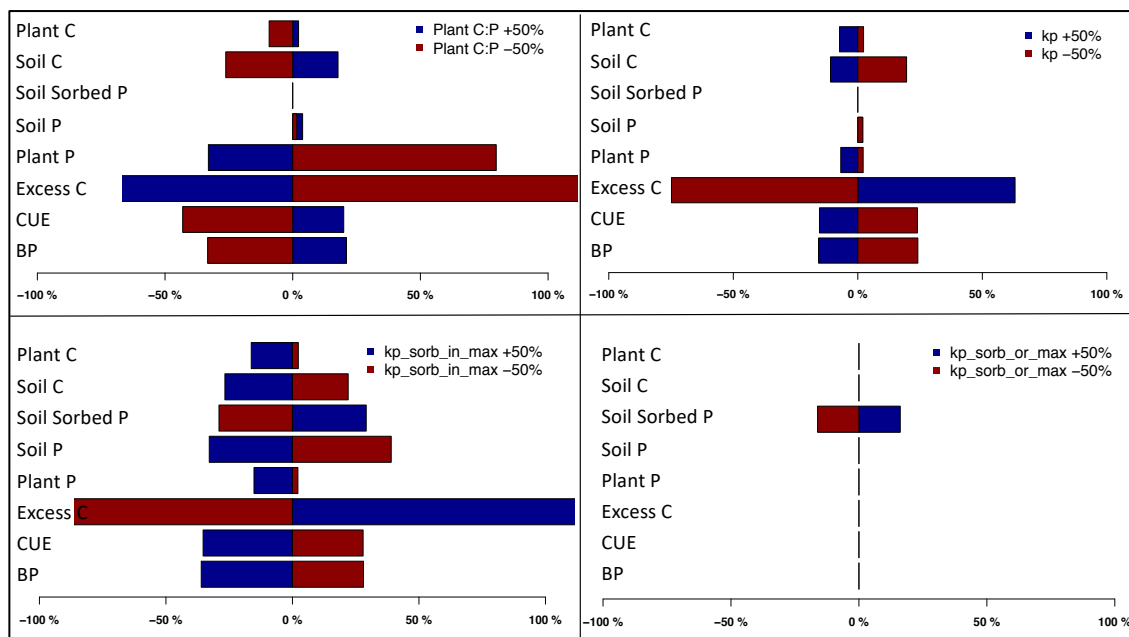


Figure. 4- Model sensitivity test results and corresponding C and P pools and fluxes under ambient CO₂.

3.2 Model application under elevated CO₂

3.2.1 Simulated plant and soil C and P pools and fluxes -JULES CNP: eCO₂ vs ambient CO₂

The eCO₂ simulation using JULES CNP yields a higher GPP compared to the ambient CO₂ (0.83 (kg C m⁻² yr⁻¹) increase), as a result of CO₂ fertilization. Moreover, due to the GPP increase, NPP and RESP follows the same trend and increased compared to ambient CO₂ (NPP: 0.49 and RESP:0.3 (kg C m⁻² yr⁻¹) increase) (Table 5). The total simulated vegetation C pool increases under eCO₂ compared to ambient CO₂ (0.41 kg C m⁻²), hence the estimated plant P (estimated as a fraction of C:P ratios) increases as well (+0.45 (g P m⁻²)) (Fig 6, Table 4). Thus, the simulated plant P demand is higher, and as the total available soil P for uptake is limited, the simulated excess C flux increases to 0.51(kg C m⁻² yr⁻¹). Moreover, despite the higher NPP under eCO₂ compared to simulated NPP under ambient CO₂, due to the substantial increase in simulated excess C, the BP is similar to the ambient CO₂ (2% difference).

709 The simulated organic soil P under eCO₂ yields close to the ambient CO₂ (1.6 g P m⁻²) (Table 5). This is due to
 710 the same parameterization of the output fluxes from this pool for eCO₂ and ambient CO₂. The simulated pool of
 711 inorganic P under eCO₂ decreases compared to the ambient CO₂ by 0.11 (g P m⁻²) due to the increased plant P
 712 pools and slight increase in uptake (+0.13 %).
 713 However, the simulated sorbed organic and inorganic soil P from eCO₂ are similar to those simulated under the
 714 ambient CO₂ which is due to the same parameterizing of sorption function (maximum sorption capacity) from
 715 the ambient CO₂ run as explained in calibration section. Moreover, the modelled occluded and weathered soil P
 716 yield similar to those in the ambient CO₂ simulation (Table 5) which is due to the same prescribed observational
 717 data that was used for this simulation.

718 3.2.2 Comparison of JULES C, CN and CNP under elevated CO₂

720 JULES C/CN show higher vegetation and soil C pools, BP and litter flux compared to JULES-CNP: (Table 6,
 721 Figure. S2). Under eCO₂, simulated NPP using JULES C-CN is 4.5% higher than JULES CNP and the BP with
 722 JULES- C/CN is 96.8% higher than in JULES-CNP which simulates an [excess C](#) flux of 0.81 (kg C m⁻² yr⁻¹)
 723 equivalent to 46% P limitation under eCO₂. As a result of P limitation and eCO₂, the simulated CO₂ fertilization
 724 effect estimated based on changes in biomass under ambient and eCO₂ was reduced from 13% with JULES-
 725 C/CN to 10% JULES-CNP. Moreover, the CUE from JULES C/CN is 87.5% higher than the JULES CNP as a
 726 result of high P limitation over biomass production.
 727

728
 729 **Table 6.** C pools and fluxes using JULES C/CN and difference in percentage with JULES CNP model under eCO₂. A
 730 positive % means larger respective values simulated with JULES C and JULES CN than with JULES CNP (between period
 731 2017-18).

	GPP	NPP	BP	CUE	Litter C	Leaf C	Root C	Wood C	Soil C
JULES C/CN	4.1	1.85	1.85	45%	1.77	0.42	0.42	26.1	19.2
JULES CNP	3.9	1.77	0.94	24%	0.83	0.4	0.4	24.71	12.71
ΔC/CN: CNP	5.1%	4.5%	96.8%	87.5%	113.3%	5%	5%	5%	51.1%

732 3.2.2.1 Inter-models under elevated CO₂

733 Following Fleischer *et al.*, (2019), we report the simulated response to eCO₂ for year 1999 (initial: CO₂ effect)
 734 and 1999-2013 (15 years: final effect) which are different than our evaluation period (2017-18). Using JULES C
 735 and JULES CN under eCO₂, simulated GPP and NPP during the 1st year increase by 30% and 61% respectively
 736 and by 28% and 52% after 15 years (Figure. 5). However, using JULES CNP, eCO₂ increases simulated GPP,
 737 NPP and BP responses during the 1st year by 29%,51% and 20% and by 28%, 43% and 7%, after 15 years
 738 respectively.
 739

740 Corresponding simulated CUE during the 1st year and 15 years shows an increase of 24% and 20% in response
 741 to eCO₂ using JULES C/CN respectively. However, using JULES CNP, simulated CUE for the 1st and after 15
 742 years is reduced by 7% and 17% in response to eCO₂.
 743

744 Simulated total biomass (leaf, fine root and wood C) (ΔC_{veg}) using JULES C/CN for the 1st and 15 years of
 745 eCO₂ increases by 9% and 13% respectively. However, using JULES CNP ΔC_{veg} only increases by 0.5% and
 746 9% for 1st and 15 years of eCO₂, respectively.
 747
 748
 749
 750

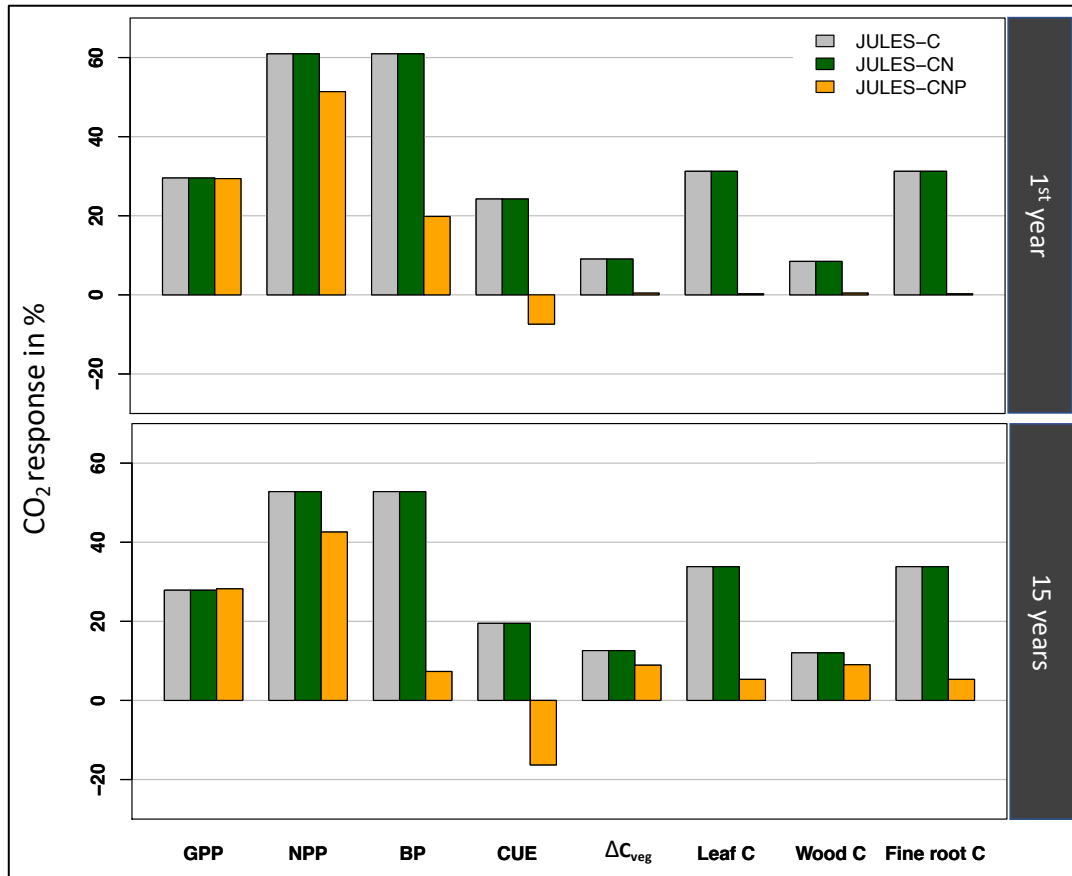


Figure. 5- Relative effect of eCO₂ on simulated GPP, NPP, BP, CUE, ΔC_{veg}, leaf C and fine root C, using three versions of JULES model in 1st (initial response) and 15 years periods (final response).

3.3 Plant P Demand, uptake and [excess C](#) under ambient and elevated CO₂

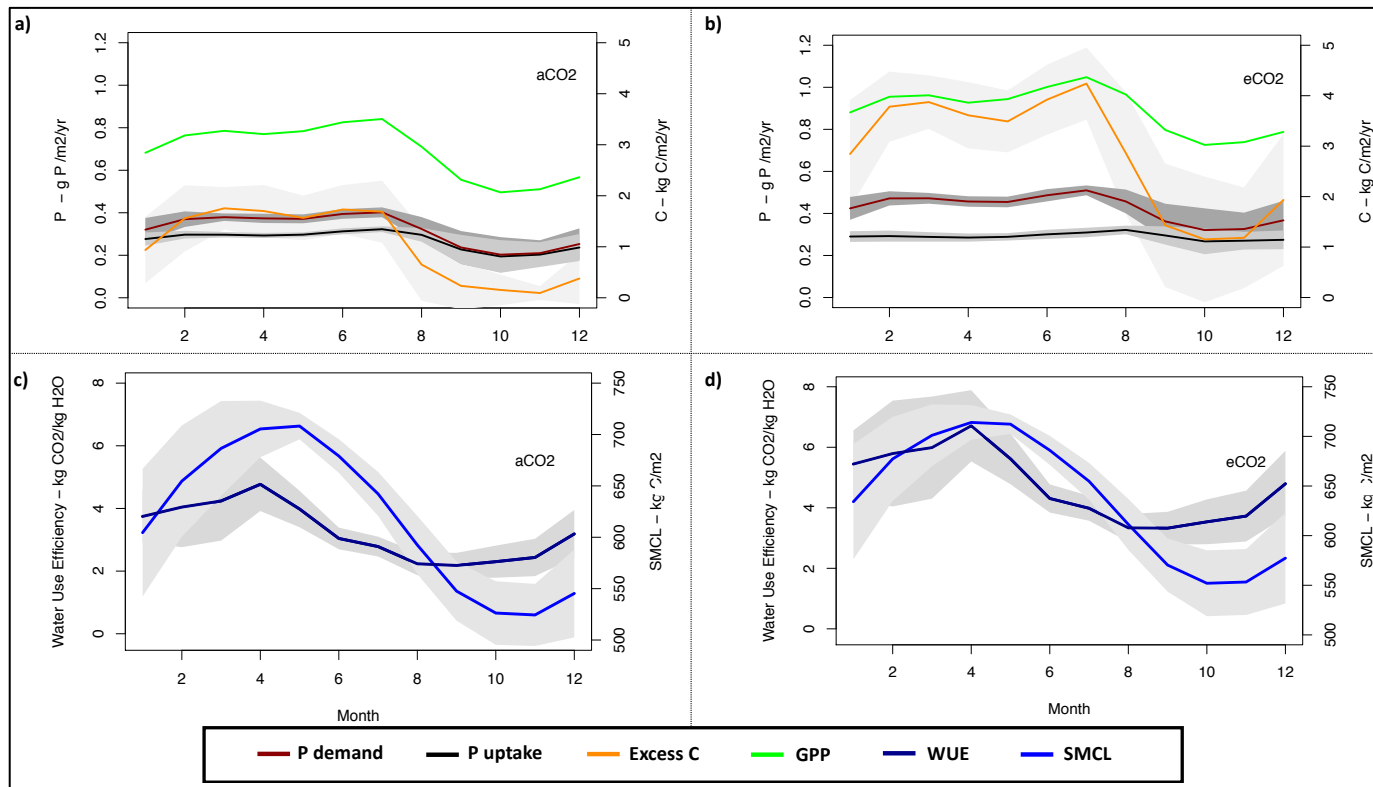
To understand further the CP-cycle dynamics, we studied the monthly averaged plant P demand and the relative (limited) P uptake (eq. 26) under both ambient and elevated CO₂ conditions (Figure. 6).

Under ambient CO₂ condition the highest GPP is estimated at $3.5 \pm 0.19 \text{ kg C m}^{-2} \text{ month}^{-1}$ in July and the lowest at $2.06 \pm 0.61 \text{ kg C m}^{-2} \text{ month}^{-1}$ in October (Figure. 6-a). The estimated WUE and SMCL in October is among the lowest estimated monthly values at $2.3 \pm 0.51 \text{ kg CO}_2/\text{kg H}_2\text{O}$ and $526.2 \pm 31 \text{ kg m}^{-2}$ respectively (Figure. 6-c). The highest P demand is estimated at $0.4 \pm 0.02 \text{ g P m}^{-2} \text{ month}^{-1}$ in July and the lowest demand at $0.2 \pm 0.08 \text{ g P m}^{-2} \text{ month}^{-1}$ in October. Consequently, the highest and lowest uptake (0.32 ± 0.01 and $0.19 \pm 0.07 \text{ g P m}^{-2} \text{ month}^{-1}$, respectively). The [excess C](#) for the highest and lowest GPP and demand periods are estimated at 0.4 ± 15 and $0.04 \pm 0.07 \text{ kg C m}^{-2} \text{ month}^{-1}$, respectively.

However, similar to ambient CO₂, under eCO₂ condition the highest estimated GPP is in July at $4.36 \pm 0.21 \text{ kg C m}^{-2} \text{ month}^{-1}$ and lowest for October $3.02 \pm 0.75 \text{ kg C m}^{-2} \text{ month}^{-1}$ (Figure. 6-b). The estimated WUE and [soil moisture content \(SMCL\)](#) for the lowest GPP period is among the lowest monthly estimated values at $3.5 \pm 0.74 \text{ kg CO}_2/\text{kg H}_2\text{O}$ and $552 \pm 33 \text{ kg m}^{-2}$ for October respectively (Figure. 6-d). The highest P demand is estimated for July at $0.51 \pm 0.02 \text{ g P m}^{-2} \text{ month}^{-1}$ with the uptake flux of $0.31 \pm 0.02 \text{ g P m}^{-2} \text{ month}^{-1}$ and the lowest demand is estimated for October at $0.32 \pm 0.1 \text{ g P m}^{-2} \text{ month}^{-1}$ with the estimated uptake flux of $0.26 \pm 0.06 \text{ g P m}^{-2} \text{ month}^{-1}$. The highest [excess C](#) flux is also for July at $1.01 \pm 0.17 \text{ kg C m}^{-2} \text{ month}^{-1}$ and lowest for October $0.27 \pm 0.29 \text{ kg C m}^{-2} \text{ month}^{-1}$, respectively.

However, despite the P limitation in both eCO₂ and ambient CO₂ conditions, the P uptake flux under eCO₂ is higher than the ambient CO₂ condition. This is due to the higher WUE and increased SMCL (controlling uptake capacity (eq. 27)) under eCO₂ condition, hence more water availability during the dry season to maintain productivity and critically transport P to the plant (see eq. 27), compared to ambient CO₂ condition (Figure. 6-c and d). [Additionally, in JULES both the vertical discretisation \(Burke, Chadburn and Ekici, 2017\) and](#)

783 [mineralisation terms \(Wiltshire *et al.*, 2021\) depend on the soil moisture and temperature. Thus, higher P](#)
 784 [concentration and uptake under eCO₂ condition.](#)
 785



786
 787 **Figure 6-** Simulated monthly plant P demand and uptake ($\text{g P m}^{-2} \text{ yr}^{-1}$), excess C and GPP ($\text{kg C m}^{-2} \text{ yr}^{-1}$) under a) aCO₂
 788 and b) eCO₂, water use efficiency ($\text{g m}^{-2} \text{ yr}^{-1}$) under c) ambient CO₂ (aCO₂) and d) eCO₂ conditions. The grey area represents
 789 the standard deviation.
 790

791 3.4 Soil P pools profile under ambient CO₂ and elevated CO₂

792 We explored the distribution of the inorganic and organic soil P and their sorbed fraction within the soil layers
 793 and under different CO₂ conditions (Figure. S3). Both the ambient and eCO₂ simulations have a close inorganic
 794 soil P distribution at the topsoil layer (0-30cm) (0.85 vs. 0.9 (g P m^{-2}) respectively) as well as similar organic
 795 soil P distribution (0.85 vs 0.9 (g P m^{-2}) respectively).
 796

797 However, the organic soil P and sorbed forms of inorganic and organic soil P profiles are not changing
 798 significantly between different sets due to the similar parameterization of the processes that control these pools
 799 (processes which are related to the physical aspects of soils, hence not changing under eCO₂ condition) and the
 800 same parameter values used for both ambient and eCO₂ runs.
 801

802 Moreover, the soil P within 30cm soil depth for ambient and eCO₂ conditions is at 14.7 (g P m^{-2}) and 14.56 (g P
 803 m^{-2}) respectively, and the total ecosystem P for both ambient and eCO₂ conditions is at 35.97 (g P m^{-2}).
 804 However, the slightly lower soil P in the eCO₂ condition is due to the higher plant P demand compared to the
 805 ambient condition, hence the higher allocated P vegetation (10%) under eCO₂ condition.
 806

807 4. Discussion

808 Studies show the significant role of the tropical forests, and Amazonia in particular, in C uptake and regulating
 809 atmospheric CO₂ (Brienen *et al.*, 2015; Phillips *et al.*, 2017). [As soil P availability is low in the majority of](#)
 810 [Amazonia \(Quesada *et al.*, 2012\), the competition for nutrients by both plant and soil communities is high](#)
 811 [\(Lloyd *et al.*, 2001\). The responses of these communities to eCO₂ under P limited conditions remains uncertain](#)
 812 [\(Fleischer *et al.*, 2019\). These responses in P enabled models are represented in different ways regarding the](#)
 813 [excess C which is not used for plant growth due to P limitation. Either growth is directly downregulated taking](#)
 814 [the minimum labile plant C,N and P \(Goll *et al.*, 2017\), or photosynthesis is downregulated via \$V_{\text{cmax}}\$ and \$J_{\text{max}}\$](#)
 815

(Comins and McMurtrie, 1993; Yang *et al.*, 2014; Zhu *et al.*, 2016) and finally models like JULES CNP downregulate NPP via respiration of excess carbon that cannot be used for growth due to plant nutrient constraints (Haverd *et al.*, 2018). The estimated CUE depends on the modelling approach. Models that down regulate the photosynthetic capacity and GPP consequently (Comins and McMurtrie, 1993; Yang *et al.*, 2014; Zhu *et al.*, 2016), simulate a positive CUE response to CO₂ fertilization while models that down regulate the NPP and respire the excess C (Haverd *et al.*, 2018) simulate a negative CUE response (Fleischer *et al.*, 2019) which is in line with the studies showing lower CUE when nutrient availability declines (Vicca *et al.*, 2012). However, this remains a major uncertainty in understanding the implication of P limitation on terrestrial biogeochemical cycles. Our new developments include major P processes in both plant and soil pools and can be applied to the Amazon region using existing soil (Quesada *et al.*, 2011) and foliar structural and nutrient (Fyllas *et al.*, 2009) data for parameterisation. Moreover, JULES CNP can be applied at the global scale and for future projections using global soil P data (Sun *et al.*, 2021) for model initialization and PFT-specific plant stoichiometries (Zechmeister-Boltenstern *et al.* 2015), soil stoichiometries (Zechmeister-Boltenstern *et al.* 2015; Tipping *et al.* (2016), sorption and weathering ratios (based on lithological class specific from the GliM lithological map (Hartmann and Moosdorf, 2012) and soil shielding from Hartmann *et al.*, (2014)).

4.1. Evaluation of model performance against observations

JULES-CNP could reproduce the magnitude of soil organic and inorganic P pools and fluxes. The relative distribution of total organic P, total inorganic P and residue P fractions of total P in soils under Brazilian Eucalyptus plantations (Costa *et al.*, 2016) shows inorganic P fraction of 28% from total soil P which is close to our estimation of 24% and organic P fraction of 30% from total soil P which is higher than our estimated fraction of 18%. Thus, we may need to improve the process representation or parameters that control the organic P concentration, such as litter flux and decomposition, soil organic P mineralization, and immobilization in the future.

Our estimated maximum P uptake, which represents the actual available P for plant uptake (Goll *et al.*, 2017), for both ambient and eCO₂ conditions, is highly correlated with the plant P demand ($R^2 = 0.96$ and 0.52 respectively). The plant P demand depends on the GPP changes which are reflected by the WUE (Hatfield and Dold, 2019). Hence, under ambient CO₂, JULES CNP simulates lower GPP and plant P demand during the dry season than during the wet season. Sufficient P uptake during these periods results in the lowest P limitation, thus the lowest simulated excess C. Nevertheless, under eCO₂ the same pattern is simulated but a higher availability of soil P due to the stomatal closure in the dry season. Hence, due to the plant's more efficient water usage, the soil moisture in the dry season is higher (Xu *et al.*, 2016) which impacts our capped P uptake flux (eq. 27) and increases the uptake capacity respectively.

Overall, JULES-CNP reproduced the observed C pools and fluxes which are in the acceptable ranges compared to the measurements. However, using the JULES default V_{cmax} estimation method (eq. 40), the model slightly underestimates the total GPP ($2.9 \text{ kg C m}^{-2} \text{ yr}^{-1}$ vs. $3\text{-}3.5 \text{ kg C m}^{-2} \text{ yr}^{-1}$). Therefore, in this version of the model, we used the improved V_{cmax} estimation method based on N and P (eq. 46) which resulted a final estimated GPP closer to the measurements ($3.06 \text{ kg C m}^{-2} \text{ yr}^{-1}$).

Our results show an increase in GPP (21%) in response to eCO₂ which is higher than the average increase of GPP reported in mature eucalyptus forests (11%), also growing under low P soils at the free air CO₂ enrichment experiment (EucFACE) facility in Australia (Jiang *et al.*, 2020). This can be related to the lower decrease of biomass growth response estimated by JULES-CNP (-3%) compared to the measurements from mature forests (-8%) (Ellsworth *et al.*, 2017), due to the P limitation which showed to impact the above-ground biomass growth response in mature forests (Körner *et al.*, 2005; Ryan, 2013; Klein *et al.*, 2016).

In order to estimate the biomass production (BP), we deducted the excess C fluxes from the NPP. Using JULES C/CN models our estimated biomass productivity enhancement due to eCO₂ (49%) is in the middle range of the reported various studies from different biomes by Walker *et al.*, (2021). Moreover, our estimated difference of BP between ambient and eCO₂ conditions (2%) is close to the estimated difference for mature forests (3%) (Jiang *et al.*, 2020).

A global estimation for tropical forests using CASACNP model which includes N and P limitations on terrestrial C cycling, shows that NPP is reduced by 20% on average due to the insufficient P availability (Wang, Law and Pak, 2010) which is close to our estimated P limitation of 24%. This finding is in line with experimental study that shows a strong correlation between the total NPP and the soil available P (Aragão *et al.*, 2009). Nevertheless, our model show that the P limitation mimics the same response to the CO₂ fertilization

878 similar to sites in pool soils (see ZAR-01 site in Aragão *et al.*, (2009)). The estimated decrease of NPP in
879 response to eCO₂ as a result of P limitation is in line with the findings from CLM-CNP model at five tropical
880 forests (Yang *et al.*, 2014) which indicates the CO₂ fertilization dependency on the processes that affect P
881 availability or uptake.

882
883 Our estimated CUE (0.31) is close to the estimation by Jiang *et al.* (2020) for mature forests (0.31±0.03), as well
884 as to the measurement for our study site (0.34±0.1). There is currently a lack of representation of stand age in
885 JULES-CNP which can significantly change this ratio (e.g. mature trees are less responsive to the nutrient
886 limitations) (De Lucia *et al.*, 2007; Norby *et al.*, 2016). However, a recent development of Robust Ecosystem
887 Demography (RED) model into JULES (Argles *et al.*, 2020) and its integration into JULES-CNP in the future
888 can resolve this issue. Moreover under low P availability, all available P is considered to be adsorbed or taken
889 by plant and microbes for further consumption, with leaching considered to be minor within the time scales of
890 our study period (Went and Stark, 1968; Bruijnzeel, 1991; Neff, Hobbie and Vitousek, 2000).
891 Due to the strong fixation of P in the soil (Aerts & Chapin, 2000; Goodale, Lajtha, Nadelhoffer, Boyer, &
892 Jaworski, 2002), the P deposited is unlikely to be available to plants in the short term (de Vries *et al.*, 2014), for
893 this reason this version of JULES CNP did not include P deposition. However both P deposition and leaching
894 are likely to have a very important role on sustaining the productivity of tropical forests in the Amazon over
895 longer time scales (Van Langenhove *et al.*, 2020) and needs to be considered in future studies.
896 Moreover, biochemical mineralisation is not included in the current version of JULES CNP and it only accounts
897 for total mineralization. However, even the models which includes this process, show no significant difference
898 between total and biochemical mineralized P which can be due to complexity of identifying the inclination of
899 mineralization versus uptake (Martins *et al.*, 2021).
900 Lastly, in order to capture plant internal nutrient impact on the C storage, the future work should focus on
901 implanting a recent developed Non-Structural Carbohydrate (NSC) model (SUGAR) (Jones *et al.*, 2020) in
902 JULES-CNP.

903 904 **4.2. Inter-models comparison**

905
906 The comparison of simulated GPP enhancement across JULES versions for the 1st year is within the middle
907 range of the 1st year CO₂ responses of the C/CN models studied by Fleischer *et al.*, (2019) evaluating simulated
908 eCO₂ effects at a site in Manaus using the same meteorological forcing and methodology used in this study for
909 a range of DGVM's. However, comparison for 15 years of eCO₂, shows that the simulated response with
910 JULES CNP is on the higher end of Fleischer *et al.*, (2019) study which is due to the higher estimated biomass
911 growth by JULES CNP (Table S1). Similarly, using JULES CNP our estimated GPP enhancement is on the
912 higher end of model estimations in Fleischer *et al.*, (2019). Moreover, comparing the GPP responses between
913 different versions of (JULES C/CN and CNP), the JULES CNP shows a slightly higher response to CO₂
914 fertilization associated with the higher WUE changes (Xiao *et al.*, 2013) (Figure. S4). This is due to the higher
915 sensitivity of the plant to water availability than the P availability in the P limited system (He and Dijkstra,
916 2014). Hence, under eCO₂ due to water-saving strategy of plants and stomatal closure (Medlyn *et al.*, 2016),
917 simulated transpiration is decreased (Sampaio *et al.*, 2021) and photosynthesis is enhanced compared ambient
918 CO₂.

919
920 To that end, the monthly changes of WUE in JULES CNP are highly correlated to the GPP, hence the lowest
921 and highest WUE follow the same periods as GPP similar to responses captured with models studied by
922 Fleischer *et al.*, (2019) (Table. S1).

923
924 Our estimated NPP enhancement using JULES C/CN models for both 1st and 15 years period is within the
925 middle range of the models in Fleischer *et al.*, (2019). Nevertheless, JULES CNP response of BP is in the lower
926 band of the CNP models by Fleischer *et al.*, (2019) and close to the estimations from CABLE (Haverd *et al.*,
927 2018) and ORCHIDEE (Goll *et al.*, 2017) models, which may be due to the similar representation of P processes
928 and limitation between these models. However, our results show a 29% decrease in NPP using JULES-CNP
929 compared to JULES-C/CN which is smaller than the differences between the CLM-CNP and CLM-CN versions
930 (51% decrease) (Yang *et al.*, 2014). The lower estimated decrease in JULES highlights the need to further study
931 the fully corresponding plant C pools and fluxes to the changes in soil and plant P. Therefore, future work
932 should be focused on the improvement of the total P availability and the plant C feedbacks. Moreover, there are
933 other environmental factors such as temperature which shows a possible impact on the CO₂ elevation and the
934 changes of NPP (Baig *et al.*, 2015) which needs further improvement in our model.

935 The CUE estimations of 1st year and 15 years response to CO₂ elevation from JULES C/CN are in the middle
936 range of C/CN models in Fleischer *et al.*, (2019). However, the estimated CUE using JULES CNP for 1st and 15

937 years are in the low range of CNP models reported by Fleischer *et al.*, (2019) which is due to the same reason
938 discussed for NPP comparison.
939

940 Finally, our estimated total biomass enhancement (ΔC_{veg}) using JULES C/CN for the 1st and 15 years are in the
941 middle range of C/CN models from Fleischer *et al.*, (2019) and in lower range of CNP models from Fleischer *et al.*
942 *et al.*, (2019) using JULES CNP. Nevertheless, while JULES-CNP includes the trait-based parameters (Harper *et al.*
943 *et al.*, 2016), other functions such as flexible C allocation and spatial variation of biomass turnover are still
944 missing and future model improvement should be focused on their inclusion.
945

946 5. Conclusion

947 Land ecosystems are a significant sink of atmospheric CO₂, ergo buffering the anthropogenic increase of this
948 flux. While tropical forests contribute substantially to the global land C sink, observational studies show that a
949 stalled increase in carbon gains over the recent decade (Brienen *et al.*, 2015; Hubau *et al.*, 2020). However
950 modelling studies that lack representation of P cycling processes predict an increasing sink (Fernández-Martínez
951 *et al.*, 2019; Fleischer *et al.*, 2019). This is particularly relevant for efforts to mitigate dangerous climate change
952 and assumptions on the future efficacy of the land C sink. Therefore, in this study, we presented the full
953 terrestrial P cycling and its feedback on the C cycle within the JULES framework. Our results show that the
954 model is capable of representing plant and soil P pools and fluxes at a site in Central Amazon. Moreover, the
955 model estimated a significant NPP limitation under ambient CO₂, due to the high P deficiency at this site which
956 is representative of Central Amazon, and elevated CO₂ resulted in a further subsequent decrease in the land C
957 sink capacity relative to the model without P limitation. While our study is a [step toward the](#) full nutrient cycling
958 representation in ESMs, it can also help the empirical community to test different hypotheses (i.e., dynamic
959 allocation and stoichiometry) and generate targeted experimental measurements (Medlyn *et al.*, 2015).
960

961 [Code availability](#)

962 The modified version of JULES vn5_5 and the P extension developed for this paper [are freely available on](#) Met
963 Office Science Repository Service:
964 https://code.metoffice.gov.uk/svn/jules/main/branches/dev/mahdinakhavali/vn5.5_JULES_PM_NAKHAVALI/
965 [after registration \(http://jules-lsm.github.io/access_req/JULES_access.html\)](http://jules-lsm.github.io/access_req/JULES_access.html) and [completion of software license](#)
966 [form](#). Codes for compiling model available at: (<https://doi.org/10.5281/zenodo.5711160>). Simulations were
967 conducted using two sets of model configurations (namelists): ambient CO₂ condition
968 (<https://doi.org/10.5281/zenodo.5711144>) and elevated CO₂ condition
969 (<https://doi.org/10.5281/zenodo.5711150>).
970

971 [Data availability](#)

972 The model outputs related to the results in this paper are provided on Zenodo repository
973 (<https://doi.org/10.5281/zenodo.5710898>). All the R scripts used for processing the model outputs and
974 producing results in form of table or figures are provided on Zenodo repository
975 (<https://doi.org/10.5281/zenodo.5710896>).

976 *Author contributions.* MAN, LMM, SS, SEC, CAQ, AJW, IAP, KMA and DBC developed the model, per-
977 formed simulations and analysis. CAQ, FVC, RP, LFL, KMA, GR, LS, ACMM, JSR, RA and JLC provided the
978 measurements for the model parasitisation and evaluation. MAN, LMM, SS, IAP, SEC, FVC, RP, LFL, KMA
979 and DBC contributed in writing the manuscript.
980

981 *Competing interests.* The authors declare no competing interests
982

983 *Acknowledgments.* This work and its contributors (MAN, LMM, KMA and IPH) were supported by the UK
984 Natural Environment Research Council (NERC) grant no NE/LE007223/1. MAN, LMM, SS, IPH were also
985 supported by the Newton Fund through the Met Office Climate Science for Service Partnership Brazil (CSSP
986 Brazil). LMM acknowledges support from the Natural Environment Research Council, grant NEC05816 LTS-
987 M-UKESM. LFL was also supported by AmazonFACE programme (CAPES) and the National Institute of
988 Amazonian Research, grant no: 88887.154643/2017-00. The authors acknowledge contributions from Celso
989 Von Randow towards data curation of the meteorological forcing used in this study and Daniel Goll for
990 modelling insight. We would like to thank Alessandro C. de Araújo and the Large-Scale Biosphere-Atmosphere
991 Program (LBA), coordinated by the National Institute for Amazon Researches (INPA), for the use and
992 availability of data.

993 **References:**

- 994
- 995 Aerts, R. and Chapin, F. S. (1999) 'The Mineral Nutrition of Wild Plants Revisited: A Re-evaluation of
- 996 Processes and Patterns', *Advances in Ecological Research*, 30(C), pp. 1–67. doi: 10.1016/S0065-
- 997 2504(08)60016-1.
- 998 Anav, A. *et al.* (2013) 'Evaluating the land and ocean components of the global carbon cycle in the CMIP5 earth
- 999 system models', *Journal of Climate*, 26(18), pp. 6801–6843. doi: 10.1175/JCLI-D-12-00417.1.
- 1000 Aragão, L. E. O. C. *et al.* (2009) 'Above- and below-ground net primary productivity across ten Amazonian
- 1001 forests on contrasting soils', *Biogeosciences Discussions*, 6(1), pp. 2441–2488. doi: 10.5194/bgd-6-2441-2009.
- 1002 Araçõ, L. E. O. C. *et al.* (2009) 'Above- and below-ground net primary productivity across ten Amazonian
- 1003 forests on contrasting soils', *Biogeosciences*, 6(12), pp. 2759–2778. doi: 10.5194/bg-6-2759-2009.
- 1004 Araújo, A. C. *et al.* (2002) 'Comparative measurements of carbon dioxide fluxes from two nearby towers in a
- 1005 central Amazonian rainforest: The Manaus LBA site', *Journal of Geophysical Research*, 107(D20), p. 8090.
- 1006 doi: 10.1029/2001JD000676.
- 1007 Argles, A. P. K. *et al.* (2020) 'Robust Ecosystem Demography (RED version 1.0): A parsimonious approach to
- 1008 modelling vegetation dynamics in Earth system models', *Geoscientific Model Development*, 13(9), pp. 4067–
- 1009 4089. doi: 10.5194/gmd-13-4067-2020.
- 1010 Arora, V. K. *et al.* (2020) 'Carbon–concentration and carbon–climate feedbacks in CMIP6 models and their
- 1011 comparison to CMIP5 models', *Biogeosciences*, 17(16), pp. 4173–4222. doi: 10.5194/bg-17-4173-2020.
- 1012 Baig, S. *et al.* (2015) 'Does the growth response of woody plants to elevated CO₂ increase with temperature? A
- 1013 model-oriented meta-analysis', *Global Change Biology*, 21(12), pp. 4303–4319. doi: 10.1111/gcb.12962.
- 1014 Baker, T. R. *et al.* (2004) 'Variation in wood density determines spatial patterns in Amazonian forest biomass',
- 1015 *Global Change Biology*, 10(5), pp. 545–562. doi: 10.1111/j.1365-2486.2004.00751.x.
- 1016 Bentsen, M. *et al.* (2013) 'The Norwegian Earth System Model, NorESM1-M – Part 1: Description and basic
- 1017 evaluation of the physical climate', *Geoscientific Model Development*, 6(3), pp. 687–720. doi: 10.5194/gmd-6-
- 1018 687-2013.
- 1019 Best, M. J. *et al.* (2011) 'The Joint UK Land Environment Simulator (JULES), model description – Part 1:
- 1020 Carbon fluxes and vegetation dynamics', *Geoscientific Model Development*, 4(3), pp. 701–722. doi:
- 1021 10.5194/gmd-4-701-2011.
- 1022 Bradford, M. A. and Crowther, T. W. (2013) 'Carbon use efficiency and storage in terrestrial ecosystems', *New*
- 1023 *Phytologist*, 199(1), pp. 7–9. doi: 10.1111/nph.12334.
- 1024 Brienen, R. J. W. *et al.* (2015) 'Long-term decline of the Amazon carbon sink', *Nature*, 519(7543), pp. 344–
- 1025 348. doi: 10.1038/nature14283.
- 1026 Bruijnzeel, L. A. (1991) 'Nutrient input—output budgets of tropical forest ecosystems: A review', *Journal of*
- 1027 *Tropical Ecology*, 7(1), pp. 1–24. doi: 10.1017/S0266467400005010.
- 1028 Burke, E. J., Chadburn, S. E. and Ekici, A. (2017) 'A vertical representation of soil carbon in the JULES land
- 1029 surface scheme (vn4.3-permafrost) with a focus on permafrost regions', *Geoscientific Model Development*,
- 1030 10(2), pp. 959–975. doi: 10.5194/gmd-10-959-2017.
- 1031 Castanho, A. D. A. *et al.* (2013) 'Improving simulated Amazon forest biomass and productivity by including
- 1032 spatial variation in biophysical parameters', *Biogeosciences*, 10(4), pp. 2255–2272. doi: 10.5194/bg-10-2255-
- 1033 2013.
- 1034 Chapin, F. S. *et al.* (2011) *Principles of Terrestrial Ecosystem Ecology*. Springer New York (Biomedical and
- 1035 Life Sciences). Available at: <https://books.google.co.uk/books?id=68nFNpceRmIC>.
- 1036 Chave, J. *et al.* (2014) 'Improved allometric models to estimate the aboveground biomass of tropical trees',
- 1037 *Global Change Biology*, 20(10), pp. 3177–3190. doi: 10.1111/gcb.12629.
- 1038 Clark, D. B. *et al.* (2011) 'The Joint UK Land Environment Simulator (JULES), model description – Part 2:
- 1039 Carbon fluxes and vegetation dynamics', *Geoscientific Model Development*, 4(3), pp. 701–722. doi:
- 1040 10.5194/gmd-4-701-2011.
- 1041 Collatz, G. J. *et al.* (1991) 'Physiological and environmental regulation of stomatal conductance, photosynthesis
- 1042 and transpiration: a model that includes a laminar boundary layer', *Agricultural and Forest Meteorology*, 54(2–
- 1043 4), pp. 107–136. doi: 10.1016/0168-1923(91)90002-8.
- 1044 Collatz, G., Ribas-Carbo, M. and Berry, J. (1992) 'Coupled Photosynthesis-Stomatal Conductance Model for
- 1045 Leaves of C₄ Plants', *Functional Plant Biology*, 19(5), p. 519. doi: 10.1071/pp9920519.
- 1046 Comins, H. N. and McMurtrie, R. E. (1993) 'Long-Term Response of Nutrient-Limited Forests to CO₂
- 1047 Enrichment; Equilibrium Behavior of Plant-Soil Models', *Ecological Applications*, 3(4), pp. 666–681. doi:
- 1048 10.2307/1942099.
- 1049 Costa, M. G. *et al.* (2016) 'Labile and Non-Labile Fractions of Phosphorus and Its Transformations in Soil
- 1050 under Eucalyptus', pp. 1–15. doi: 10.3390/f7010015.
- 1051 DeLuca, T. H., Keeney, D. R. and McCarty, G. W. (1992) 'Effect of freeze-thaw-events on mineralization of
- 1052 soil nitrogen', *Biol. Fertil. Soils*, 14, pp. 116–120. doi: 10.1007/BF00336260.

1053 Ellsworth, D. S. *et al.* (2017) ‘Elevated CO₂ does not increase eucalypt forest productivity on a low-phosphorus
1054 soil’, *Nature Climate Change*, 7(4), pp. 279–282. doi: 10.1038/nclimate3235.

1055 Elser, J. J. *et al.* (2007) ‘Global analysis of nitrogen and phosphorus limitation of primary producers in
1056 freshwater, marine and terrestrial ecosystems’, *Ecology Letters*, 10(12), pp. 1135–1142. doi: 10.1111/j.1461-
1057 0248.2007.01113.x.

1058 Fernández-Martínez, M. *et al.* (2019) ‘Global trends in carbon sinks and their relationships with CO₂ and
1059 temperature’, *Nature Climate Change*, 9(1), pp. 73–79. doi: 10.1038/s41558-018-0367-7.

1060 Fleischer, K. *et al.* (2019) ‘Amazon forest response to CO₂ fertilization dependent on plant phosphorus
1061 acquisition’, *Nature Geoscience*. doi: 10.1038/s41561-019-0404-9.

1062 Friedlingstein, P. *et al.* (2006) ‘Climate-carbon cycle feedback analysis: Results from the C4MIP model
1063 intercomparison’, *Journal of Climate*, 19(14), pp. 3337–3353. doi: 10.1175/JCLI3800.1.

1064 Friedlingstein, P. *et al.* (2019) ‘Comment on “The global tree restoration potential”’, *Science*. doi:
1065 10.1126/science.aay8060.

1066 Fyllas, N. M. *et al.* (2009) ‘Basin-wide variations in foliar properties of Amazonian forest: phylogeny, soils and
1067 climate’, *Biogeosciences*, 6(11), pp. 2677–2708. doi: 10.5194/bg-6-2677-2009.

1068 Gentile, R. *et al.* (2012) ‘Effects of long-term exposure to enriched CO₂ on the nutrient-supplying capacity of a
1069 grassland soil’, *Biology and Fertility of Soils*, 48(3), pp. 357–362. doi: [http://dx.doi.org/10.1007/s00374-011-
1070 0616-7](http://dx.doi.org/10.1007/s00374-011-0616-7).

1071 Goll, D. S. *et al.* (2017) ‘A representation of the phosphorus cycle for ORCHIDEE (revision 4520)’,
1072 *Geoscientific Model Development*, 10(10), pp. 3745–3770. doi: 10.5194/gmd-10-3745-2017.

1073 Harper, A. B. *et al.* (2016) ‘Improved representation of plant functional types and physiology in the Joint UK
1074 Land Environment Simulator (JULES v4.2) using plant trait information’, *Geoscientific Model Development*,
1075 9(7), pp. 2415–2440. doi: 10.5194/gmd-9-2415-2016.

1076 Hatfield, J. L. and Dold, C. (2019) ‘Water-use efficiency: Advances and challenges in a changing climate’,
1077 *Frontiers in Plant Science*, 10(February), pp. 1–14. doi: 10.3389/fpls.2019.00103.

1078 Haverd, V. *et al.* (2018) ‘A new version of the CABLE land surface model (Subversion revision r4601)
1079 incorporating land use and land cover change, woody vegetation demography, and a novel optimisation-based
1080 approach to plant coordination of photosynthesis’, *Geoscientific Model Development*, 11(7), pp. 2995–3026.
1081 doi: 10.5194/gmd-11-2995-2018.

1082 He, M. and Dijkstra, F. A. (2014) ‘Drought effect on plant nitrogen and phosphorus: A meta-analysis’, *New
1083 Phytologist*, 204(4), pp. 924–931. doi: 10.1111/nph.12952.

1084 Hedley, M. J., Stewart, J. W. B. and Chauhan, B. S. (1982) ‘Changes in Inorganic and Organic Soil Phosphorus
1085 Fractions Induced by Cultivation Practices and by Laboratory Incubations’, *Soil Science Society of America
1086 Journal*, 46(5), pp. 970–976. doi: <https://doi.org/10.2136/sssaj1982.03615995004600050017x>.

1087 Hou, E. *et al.* (2019) ‘Quantifying Soil Phosphorus Dynamics: A Data Assimilation Approach’, *Journal of
1088 Geophysical Research: Biogeosciences*, 124(7), pp. 2159–2173. doi: 10.1029/2018JG004903.

1089 Hou, E. *et al.* (2020) ‘Global meta-analysis shows pervasive phosphorus limitation of aboveground plant
1090 production in natural terrestrial ecosystems’, *Nature Communications*, 11(1), pp. 1–9. doi: 10.1038/s41467-020-
1091 14492-w.

1092 Hubau, W. *et al.* (2020) ‘Asynchronous carbon sink saturation in African and Amazonian tropical forests’,
1093 *Nature*, 579(7797), pp. 80–87. doi: 10.1038/s41586-020-2035-0.

1094 Hungate, B. a *et al.* (2003) ‘Nitrogen and Climate Change’, *Science*, 302(November), pp. 1512–1513.

1095 Jenkinson, D. S. *et al.* (1990) ‘The turnover of organic carbon and nitrogen in soil’, *The Royal Society*,
1096 329(1255). doi: <https://doi.org/10.1098/rstb.1990.0177>.

1097 Jenkinson, D. S. and Coleman, K. (2008) ‘The turnover of organic carbon in subsoils. Part 2. Modelling carbon
1098 turnover’, *European Journal of Soil Science*, 59(2), pp. 400–413. doi: 10.1111/j.1365-2389.2008.01026.x.

1099 Ji, D. *et al.* (2014) ‘Description and basic evaluation of Beijing Normal University Earth System Model (BNU-
1100 ESM) version 1’, *Geoscientific Model Development*, 7(5), pp. 2039–2064. doi: 10.5194/gmd-7-2039-2014.

1101 Jiang, M. *et al.* (2019) ‘Towards a more physiological representation of vegetation phosphorus processes in land
1102 surface models’, *New Phytologist*, 222(3), pp. 1223–1229. doi: 10.1111/nph.15688.

1103 Jiang, M. *et al.* (2020) ‘The fate of carbon in a mature forest under carbon dioxide enrichment’, *Nature*,
1104 580(7802), pp. 227–231. doi: 10.1038/s41586-020-2128-9.

1105 Johnson, M. O. *et al.* (2016) ‘Variation in stem mortality rates determines patterns of above-ground biomass in
1106 Amazonian forests: implications for dynamic global vegetation models’, *Global Change Biology*, 22(12), pp.
1107 3996–4013. doi: 10.1111/gcb.13315.

1108 Jones, S. *et al.* (2020) ‘The impact of a simple representation of non-structural carbohydrates on the simulated
1109 response of tropical forests to drought’, *Biogeosciences*, 17(13), pp. 3589–3612. doi: 10.5194/bg-17-3589-2020.

1110 Kattge, J. *et al.* (2009) ‘Quantifying photosynthetic capacity and its relationship to leaf nitrogen content for
1111 global-scale terrestrial biosphere models’, *Global Change Biology*, 15(4), pp. 976–991. doi:
1112 <https://doi.org/10.1111/j.1365-2486.2008.01744.x>.

- 1113 Keller, M. *et al.* (2004) ‘Ecological research in the Large-scale Biosphere-Atmosphere Experiment in
1114 Amazonia: Early results’, *Ecological Applications*, 14(4 SUPPL.), pp. 3–16. doi: 10.1890/03-6003.
- 1115 Klein, T. *et al.* (2016) ‘Growth and carbon relations of mature *Picea abies* trees under 5 years of free-air CO₂
1116 enrichment’, *Journal of Ecology*, 104(6), pp. 1720–1733. doi: 10.1111/1365-2745.12621.
- 1117 Koch, A., Hubau, W. and Lewis, S. L. (2021) ‘Earth System Models Are Not Capturing Present-Day Tropical
1118 Forest Carbon Dynamics’, *Earth’s Future*, 9(5), pp. 1–19. doi: 10.1029/2020EF001874.
- 1119 Körner, C. *et al.* (2005) ‘Ecology: Carbon flux and growth in mature deciduous forest trees exposed to elevated
1120 CO₂’, *Science*, 309(5739), pp. 1360–1362. doi: 10.1126/science.1113977.
- 1121 Van Langenhove, L. *et al.* (2020) ‘Atmospheric deposition of elements and its relevance for nutrient budgets of
1122 tropical forests’, *Biogeochemistry*, 149(2), pp. 175–193. doi: 10.1007/s10533-020-00673-8.
- 1123 Lapola, D. M. and Norby, R. (2014) ‘Assessing the effects of increased atmospheric CO₂ on the ecology and
1124 resilience of the Amazon forest’, *Science plan et implementation strategy*, AMAZON FAC.
- 1125 LeBauer, D. and Treseder, K. (2008) ‘Nitrogen Limitation of Net Primary Productivity’, *Ecology*, 89(2), pp.
1126 371–379.
- 1127 Lloyd, J. *et al.* (2001) ‘Should Phosphorus Availability Be Constraining Moist Tropical Forest Responses to
1128 Increasing CO₂ Concentrations?’, in *Global Biogeochemical Cycles in the Climate System*. Elsevier, pp. 95–
1129 114. doi: 10.1016/B978-012631260-7/50010-8.
- 1130 Long, M. C. *et al.* (2013) ‘Twentieth-century oceanic carbon uptake and storage in CESM1(BGC)’, *Journal of
1131 Climate*, 26(18), pp. 6775–6800. doi: 10.1175/JCLI-D-12-00184.1.
- 1132 De Lucia, E. H. *et al.* (2007) ‘Forest carbon use efficiency: Is respiration a constant fraction of gross primary
1133 production?’, *Global Change Biology*, 13(6), pp. 1157–1167. doi: 10.1111/j.1365-2486.2007.01365.x.
- 1134 Lugli, L. F. (2013) *Estoque de nutrientes na serrapilheira fina e grossa em função de fatores edáficos em
1135 florestas do Amazonas, Brasil*. Instituto Nacional de Pesquisas da Amazônia - INPA. Available at:
1136 <https://repositorio.inpa.gov.br/handle/1/5028>.
- 1137 Lugli, L. F. *et al.* (2020) ‘Multiple phosphorus acquisition strategies adopted by fine roots in low-fertility soils
1138 in Central Amazonia’, *Plant and Soil*, 450(1–2), pp. 49–63. doi: 10.1007/s11104-019-03963-9.
- 1139 Lugli, L. F. *et al.* (2021) ‘Rapid responses of root traits and productivity to phosphorus and cation additions in a
1140 tropical lowland forest in Amazonia’, *New Phytologist*, 230(1), pp. 116–128. doi: 10.1111/nph.17154.
- 1141 Luo, Y. *et al.* (2004) ‘Progressive nitrogen limitation of ecosystem responses to rising atmospheric carbon
1142 dioxide’, *BioScience*, 54(8), pp. 731–739. doi: 10.1641/0006-3568(2004)054[0731:PNLOER]2.0.CO;2.
- 1143 Malhi, Y. *et al.* (2004) ‘The above-ground coarse wood productivity of 104 Neotropical forest plots’, *Global
1144 Change Biology*, 10(5), pp. 563–591. doi: 10.1111/j.1529-8817.2003.00778.x.
- 1145 Malhi, Y. *et al.* (2006) ‘The regional variation of aboveground live biomass in old-growth Amazonian forests’,
1146 *Global Change Biology*, 12(7), pp. 1107–1138. doi: 10.1111/j.1365-2486.2006.01120.x.
- 1147 Malhi, Y. *et al.* (2009) ‘Comprehensive assessment of carbon productivity, allocation and storage in three
1148 Amazonian forests’, *Global Change Biology*, 15(5), pp. 1255–1274. doi: 10.1111/j.1365-2486.2008.01780.x.
- 1149 Malhi, Y. (2012) ‘The productivity, metabolism and carbon cycle of tropical forest vegetation’, *Journal of
1150 Ecology*, 100(1), pp. 65–75. doi: 10.1111/j.1365-2745.2011.01916.x.
- 1151 Malhi, Y., Doughty, C. and Galbraith, D. (2011) ‘The allocation of ecosystem net primary productivity in
1152 tropical forests’, *Philosophical Transactions of the Royal Society B: Biological Sciences*, 366(1582), pp. 3225–
1153 3245. doi: 10.1098/rstb.2011.0062.
- 1154 Martins, N. P. *et al.* (2021) ‘Fine roots stimulate nutrient release during early stages of leaf litter decomposition
1155 in a Central Amazon rainforest’, *Plant and Soil*, 469(1–2), pp. 287–303. doi: 10.1007/s11104-021-05148-9.
- 1156 Medlyn, B. E. *et al.* (2015) ‘Using ecosystem experiments to improve vegetation models’, *Nature Climate
1157 Change*, 5(6), pp. 528–534. doi: 10.1038/nclimate2621.
- 1158 Medlyn, B. E. *et al.* (2016) ‘Using models to guide field experiments: a priori predictions for the CO₂ response
1159 of a nutrient- and water-limited native Eucalypt woodland’, *Global Change Biology*, 22(8), pp. 2834–2851. doi:
1160 10.1111/gcb.13268.
- 1161 Mercado, L. M. *et al.* (2011) ‘Variations in Amazon forest productivity correlated with foliar nutrients and
1162 modelled rates of photosynthetic carbon supply’, *Philosophical Transactions of the Royal Society B: Biological
1163 Sciences*, 366(1582), pp. 3316–3329. doi: 10.1098/rstb.2011.0045.
- 1164 Mitchard, E. T. A. (2018) ‘The tropical forest carbon cycle and climate change’, *Nature*, 559(7715), pp. 527–
1165 534. doi: 10.1038/s41586-018-0300-2.
- 1166 Neff, J. C., Hobbie, S. E. and Vitousek, P. M. (2000) ‘Nutrient and mineralogical control on dissolved organic
1167 C, N and P fluxes and stoichiometry in Hawaiian soils’, *Biogeochemistry*, 51(3), pp. 283–302. doi:
1168 10.1023/A:1006414517212.
- 1169 Norby, R. J. *et al.* (2016) ‘Model–data synthesis for the next generation of forest free-air <sc>CO</sc>₂
1170 enrichment (<sc>FACE</sc>) experiments’, *New Phytologist*, 209(1), pp. 17–28. doi: 10.1111/nph.13593.
- 1171 Nordin, A., Högberg, P. and Näsholm, T. (2001) ‘Soil nitrogen form and plant nitrogen uptake along a boreal
1172 forest productivity gradient’, *Oecologia*, 129(1), pp. 125–132. doi: 10.1007/s004420100698.

1173 Pan, Y. *et al.* (2011) ‘A Large and Persistent Carbon Sink in the World’s Forests’, *Science*, 333(6045), pp. 988–
1174 993. doi: 10.1126/science.1201609.

1175 Perakis, S. S. and Hedin, L. O. (2002) ‘Nitrogen loss from unpolluted South American forests mainly via
1176 dissolved organic compounds’, *Nature*, 415(6870), pp. 416–419. doi: 10.1038/415416a.

1177 Phillips, O. L. *et al.* (2004) ‘Pattern and process in Amazon tree turnover, 1976–2001’, *Philosophical
1178 Transactions of the Royal Society B: Biological Sciences*, 359(1443), pp. 381–407. doi: 10.1098/rstb.2003.1438.

1179 Phillips, O. L. *et al.* (2017) ‘Carbon uptake by mature Amazon forests has mitigated Amazon nations’ carbon
1180 emissions’, *Carbon Balance and Management*, 12(1), pp. 1–9. doi: 10.1186/s13021-016-0069-2.

1181 Quesada, C. A. *et al.* (2010) ‘Variations in chemical and physical properties of Amazon forest soils in relation to
1182 their genesis’, *Biogeosciences*, 7(5), pp. 1515–1541. doi: 10.5194/bg-7-1515-2010.

1183 Quesada, C. A. *et al.* (2011) ‘Soils of Amazonia with particular reference to the RAINFOR sites’,
1184 *Biogeosciences*, 8(6), pp. 1415–1440. doi: 10.5194/bg-8-1415-2011.

1185 Quesada, C. A. *et al.* (2012) ‘Basin-wide variations in Amazon forest structure and function are mediated by
1186 both soils and climate’, *Biogeosciences*, 9(6), pp. 2203–2246. doi: 10.5194/bg-9-2203-2012.

1187 Reed, S. C., Yang, X. and Thornton, P. E. (2015) ‘Incorporating phosphorus cycling into global modeling
1188 efforts: A worthwhile, tractable endeavor’, *New Phytologist*, 208(2), pp. 324–329. doi: 10.1111/nph.13521.

1189 Ryan, M. G. (2013) ‘Three decades of research at Flakaliden advancing whole-tree physiology, forest ecosystem
1190 and global change research’, *Tree Physiology*, 33(11), pp. 1123–1131. doi: 10.1093/treephys/tpt100.

1191 Sampaio, G. *et al.* (2021) ‘CO₂ physiological effect can cause rainfall decrease as strong as large-scale
1192 deforestation in the Amazon’, *Biogeosciences*, 18(8), pp. 2511–2525. doi: 10.5194/bg-18-2511-2021.

1193 Sanchez, P. A. (1977) ‘Properties and Management of Soils in the Tropics’, *Soil Science*, 124(3). Available at:
1194 https://journals.lww.com/soilsci/Fulltext/1977/09000/Properties_and_Management_of_Soils_in_the_Tropics.12.aspx.
1195

1196 Sardans, J., Rivas-Ubach, A. and Peñuelas, J. (2012) ‘The C:N:P stoichiometry of organisms and ecosystems in
1197 a changing world: A review and perspectives’, *Perspectives in Plant Ecology, Evolution and Systematics*, 14(1),
1198 pp. 33–47. doi: 10.1016/j.ppees.2011.08.002.

1199 Schimel, D., Stephens, B. B. and Fisher, J. B. (2015) ‘Effect of increasing CO₂ on the terrestrial carbon cycle’,
1200 *Proceedings of the National Academy of Sciences of the United States of America*, 112(2), pp. 436–441. doi:
1201 10.1073/pnas.1407302112.

1202 Shen, J. *et al.* (2011) ‘Phosphorus dynamics: From soil to plant’, *Plant Physiology*, 156(3), pp. 997–1005. doi:
1203 10.1104/pp.111.175232.

1204 Sitch, S. *et al.* (2008) ‘Evaluation of the terrestrial carbon cycle, future plant geography and climate-carbon
1205 cycle feedbacks using five Dynamic Global Vegetation Models (DGVMs)’, *Global Change Biology*, 14(9), pp.
1206 2015–2039. doi: 10.1111/j.1365-2486.2008.01626.x.

1207 Stephenson, N. L. and Van Mantgem, P. J. (2005) ‘Forest turnover rates follow global and regional patterns of
1208 productivity’, *Ecology Letters*, 8(5), pp. 524–531. doi: 10.1111/j.1461-0248.2005.00746.x.

1209 Sun, Y. *et al.* (2021) ‘Global evaluation of the nutrient-enabled version of the land surface model ORCHIDEE-
1210 CNP v1.2 (r5986)’, *Geoscientific Model Development*, 14(4), pp. 1987–2010. doi: 10.5194/gmd-14-1987-2021.

1211 Vicca, S. *et al.* (2012) ‘Fertile forests produce biomass more efficiently’, *Ecology Letters*, 15(6), pp. 520–526.
1212 doi: 10.1111/j.1461-0248.2012.01775.x.

1213 Vitousek, P. M. *et al.* (1997) ‘Human Domination of Earth Ecosystems’, *Science*, 278(5335), p. 21. Available
1214 at: <http://www.cheric.org/research/tech/periodicals/view.php?seq=257860>.

1215 Vitousek, P. M. *et al.* (2010) ‘Terrestrial phosphorus limitation: Mechanisms, implications, and nitrogen-
1216 phosphorus interactions’, *Ecological Applications*, 20(1), pp. 5–15. doi: 10.1890/08-0127.1.

1217 Vitousek, P. M. and Howarth, R. W. (1991) ‘Nitrogen limitation on land and in the sea: How can it occur?’,
1218 *Biogeochemistry*, 13(2), pp. 87–115. doi: 10.1007/BF00002772.

1219 Walker, A. P. *et al.* (2021) ‘Integrating the evidence for a terrestrial carbon sink caused by increasing
1220 atmospheric CO₂’, *New Phytologist*, 229(5), pp. 2413–2445. doi: 10.1111/nph.16866.

1221 Walker, T. W. and Syers, J. K. (1976) ‘The fate of phosphorus during pedogenesis’, *Geoderma*, 15(1), pp. 1–19.
1222 doi: 10.1016/0016-7061(76)90066-5.

1223 Wang, Y. P., Houlton, B. Z. and Field, C. B. (2007) ‘A model of biogeochemical cycles of carbon, nitrogen, and
1224 phosphorus including symbiotic nitrogen fixation and phosphatase production’, *Global Biogeochemical Cycles*,
1225 21(1), pp. 1–15. doi: 10.1029/2006GB002797.

1226 Wang, Y. P., Law, R. M. and Pak, B. (2010) ‘A global model of carbon, nitrogen and phosphorus cycles for the
1227 terrestrial biosphere’, *Biogeosciences*, 7(7), pp. 2261–2282. doi: 10.5194/bg-7-2261-2010.

1228 Went, F. W. and Stark, N. (1968) ‘Mycorrhiza’, *BioScience*, 18(11), pp. 1035–1039. doi: 10.2307/1294552.

1229 Wiltshire, A. J. *et al.* (2021) ‘Jules-cn: A coupled terrestrial carbon-nitrogen scheme (jules vn5.1)’,
1230 *Geoscientific Model Development*, 14(4), pp. 2161–2186. doi: 10.5194/gmd-14-2161-2021.

1231 Xiao, J. *et al.* (2013) ‘Carbon fluxes, evapotranspiration, and water use efficiency of terrestrial ecosystems in
1232 China’, *Agricultural and Forest Meteorology*, 182–183, pp. 76–90. doi: 10.1016/j.agrformet.2013.08.007.

1233 Xu, Z. *et al.* (2016) 'Elevated-CO₂ response of stomata and its dependence on environmental factors', *Frontiers*
1234 *in Plant Science*, 7(MAY2016), pp. 1–15. doi: 10.3389/fpls.2016.00657.
1235 Yang, X. *et al.* (2013) 'The distribution of soil phosphorus for global biogeochemical modeling',
1236 *Biogeosciences*, 10(4), pp. 2525–2537. doi: 10.5194/bg-10-2525-2013.
1237 Yang, X. *et al.* (2014) 'The role of phosphorus dynamics in tropical forests – a modeling study using CLM-
1238 CNP', *Biogeosciences*, 11(6), pp. 1667–1681. doi: 10.5194/bg-11-1667-2014.
1239 Yang, X. and Post, W. M. (2011) 'Phosphorus transformations as a function of pedogenesis: A synthesis of soil
1240 phosphorus data using Hedley fractionation method', *Biogeosciences*, 8(10), pp. 2907–2916. doi: 10.5194/bg-8-
1241 2907-2011.
1242 Zaehle, S. and Dalmonech, D. (2011) 'Carbon-nitrogen interactions on land at global scales: Current
1243 understanding in modelling climate biosphere feedbacks', *Current Opinion in Environmental Sustainability*,
1244 3(5), pp. 311–320. doi: 10.1016/j.cosust.2011.08.008.
1245 Zaehle, S. and Friend, A. D. (2010) 'Carbon and nitrogen cycle dynamics in the O-CN land surface model: 1.
1246 Model description, site-scale evaluation, and sensitivity to parameter estimates', *Global Biogeochemical Cycles*,
1247 24(1), pp. 1–13. doi: 10.1029/2009GB003521.
1248 Zhu, Q. *et al.* (2016) 'Multiple soil nutrient competition between plants, microbes, and mineral surfaces: model
1249 development, parameterization, and example applications in several tropical forests', *Biogeosciences*, 13(1), pp.
1250 341–363. doi: 10.5194/bg-13-341-2016.
1251